Ville-Valtteri Tiittanen

Magnetic stimulation using moving permanent magnets

School of Science

Thesis submitted for examination for the degree of Master of Science in Technology.

Espoo 17.4.2015

Thesis supervisor:

Academy Prof. Risto Ilmoniemi

Thesis advisor:

M.Sc. (Tech.) Lari Koponen

Aalto University
School of Science

AALTO UNIVERSITY
SCHOOL OF SCIENCE

ABSTRACT OF THE
MASTER'S THESIS

Author: Ville-Valtteri Tiittanen

Title: Magnetic stimulation using moving permanent magnets

Date: 17.4.2015 Language: English Number of pages: 6+47

Department of Neuroscience and Biomedical Engineering

Professorship: Biomedical Engineering Code: Tfy-99

Supervisor: Academy Prof. Risto Ilmoniemi

Advisor: M.Sc. (Tech.) Lari Koponen

Transcranial magnetic stimulation (TMS) is a noninvasive method used to stimulate small regions of the brain. It has clinical applications for both therapeutic and diagnostic purposes. Traditionally TMS is conducted with an electromagnetic coil. The changing electric current gives rise to a changing magnetic field, which induces an electric field in the brain. In this study, we employ moving permanent magnets to induce an electric field. Using permanent magnets for TMS could potentially remove two disadvantages of the electromagnet-based systems: acoustic noise, and heating of the coil.

The electric field from moving magnets was calculated using the spherical head model. The calculations were verified experimentally by measuring the induced electric field with a triangular detector loop. In those experiments, the magnets were dropped past the detector loop. A prototype was built with 32 magnets ($20 \times 20 \times 20$ mm, grade N52), that were rotated on a circular track at the radius of 40 cm. The rotation rate was 507 revolutions per minute. The magnets were placed on a disk in such a pattern that the rate of change of the magnetic field would be maximal at the center point.

The closest point of measurement was at 16.3 mm distance from the magnets' surface, and the peak of the induced electric field was 2.17 ± 0.10 V/m. At 20.0 mm distance, the peak of the induced electric field was 1.72 ± 0.08 V/m. These fields are not yet strong enough to trigger action potentials in the nerve cells, but they may have some applications nevertheless. For future research, we propose some improvements with which the field strength could be increased.

Keywords: Transcranial magnetic stimulation, TMS, magnetic stimulation, permanent magnet

AALTO-YLIOPISTO
PERUSTIETEIDEN KORKEAKOULU

DIPLOMITYÖN
TIIVISTELMÄ

Tekijä: Ville-Valtteri Tiittanen

Työn nimi: Magneettistimulaatio liikkuvilla kestomagneeteilla

Päivämäärä: 17.4.2015 Kieli: Englanti Sivumäärä: 6+47

Neurotieteen ja lääketieteellisen tekniikan laitos

Professuuri: Lääketieteellinen tekniikka Koodi: Tfy-99

Valvoja: Akatemiaprofessori Risto Ilmoniemi

Ohjaaja: DI Lari Koponen

Transkraniaalinen magneettistimulaatio (TMS) on ei-invasiivinen menetelmä, jolla voidaan stimuloida pieniä aivoalueita. Sitä voidaan käyttää kliinisesti sekä diagnosointiin että terapiaan. Perinteisesti TMS:ään käytetään sähkömagneettista kelaa. Muuttuva sähkövirta synnyttää muuttuvan magneettikentän, joka indusoi aivoihin sähkökentän. Tässä tutkimuksessa käytämme liikkuvia kestomagneetteja indusoimaan sähkökentän. Kestomagneeteilla tehtävällä aivostimulaatiolla voitaisiin mahdollisesti päästä eroon kahdesta sähkömagneetteihin perustuvan TMS:n ongelmasta: häiritsevästä äänestä ja kelan kuumenemisesta.

Liikkuvien magneettien tuottama sähkökenttä laskettiin käyttäen pallomallia. Laskennan tulokset tarkistettiin kokeellisesti, mittaamalla indusoitunut sähkökenttä kolmion muotoisella virtasilmukalla. Näissä kokeissa magneetti pudotettiin virtasilmukan ohitse. Tutkimuksen seuraavassa vaiheessa rakennettiin prototyyppi, jossa käytettiin 32 magneettia ($20 \times 20 \times 20$ mm, luokka N52), joita pyöritettiin ympyräradalla 40 cm:n säteellä. Kierrosnopeus oli 507 kierrosta minuutissa. Magneetit aseteltiin levylle siten, että magneettikentän muutosnopeus olisi mahdollisimman suuri levyn keskipisteessä.

Lähin mittauspiste oli 16.3 mm etäisyydellä magneettien pinnasta, ja indusoituneen sähkökentän huippuarvo oli 2.17 ± 0.10 V/m. Mentäessä 20.0 mm etäisyydelle, huipun suuruus oli 1.72 ± 0.08 V/m. Nämä kentät eivät ole vielä tarpeeksi suuria aiheuttaakseen aktiopotentiaaleja hermosoluissa. Niillä saattaa siitä huolimatta olla joitakin sovelluksia. Myöhempää tutkimusta varten ehdotamme parannuksia, joilla kentän suuruutta voitaisiin kasvattaa.

Avainsanat: Transkraniaalinen magneettistimulaatio, TMS, magneettistimulaatio, kestomagneetti

Acknowledgements

I would like to thank Risto Ilmoniemi, my supervisor, for this interesting research topic, and for his guidance and useful critiques. I would also like to thank my thesis advisor Lari Koponen and my colleague Jaakko Nieminen for their ideas and practical assistance in conducting the experiments.

Special thanks to Jouni Pekkarinen and the Department of Engineering Design and Production, for offering their facilities and machinery to our use.

Espoo 17.4.2015

Ville-Valtteri Tiittanen

Contents

Abstract ii

Abstract (in Finnish) iii

Acknowledgements iv

Contents v

Abbreviations vi

1 Introduction 1
- 1.1 Transcranial magnetic stimulation . . . 1
- 1.2 Disadvantages of present systems . . . 3
- 1.3 Desirable electric field strength for TMS . . . 4
- 1.4 Applications for low-strength fields . . . 7

2 Mathematical methods 10
- 2.1 Calculating the induced electric field in the brain . . . 10
- 2.2 Measuring the induced electric field . . . 12
- 2.3 Measuring the magnetic moment of a magnet . . . 13

3 Verification of calculations with drop tests 15
- 3.1 Tools . . . 15
- 3.2 Methods . . . 17
- 3.3 Results . . . 19
- 3.4 Comparison of measurements and calculations . . . 23

4 A prototype with stronger electric field 25
- 4.1 Magnets and their magnetic moments . . . 25
- 4.2 Comparison of some possible magnet layouts . . . 25
- 4.3 Moving the magnet . . . 27
- 4.4 Results . . . 32
- 4.5 Suggested improvements for the future . . . 37

5 Conclusions 43

References 44

Abbreviations

AC	Alternating current
DC	Direct current
EEG	Electroencephalography
MRI	Magnetic resonance imaging
RC circuit	A resistor–capacitor circuit
tCS	Transcranial current stimulation
TMS	Transcranial magnetic stimulation

1 Introduction

1.1 Transcranial magnetic stimulation

Transcranial magnetic stimulation (TMS) is a noninvasive method used to stimulate small regions of the brain. It is based on electromagnetic induction. An external magnetic field is used to induce currents in the nerve cells of the brain. TMS was first used on human brain by Barker *et al.* in 1985 [1], so it is a relatively new technique in neuroscience. For comparison, the first human EEG was recorded by Berger in 1924 [2].

Clinically, TMS is used for therapeutic and diagnostic purposes. TMS can, for example, cause long-lasting inhibitory or excitatory effects in the targeted brain areas, which can be used for the treatment of depression [3]. Diagnostic purposes include locating lesions in the brain and locating the important areas before a surgery [4]. Transcranial magnetic stimulation has not been found to cause short- or long-term brain damage of any kind [3].

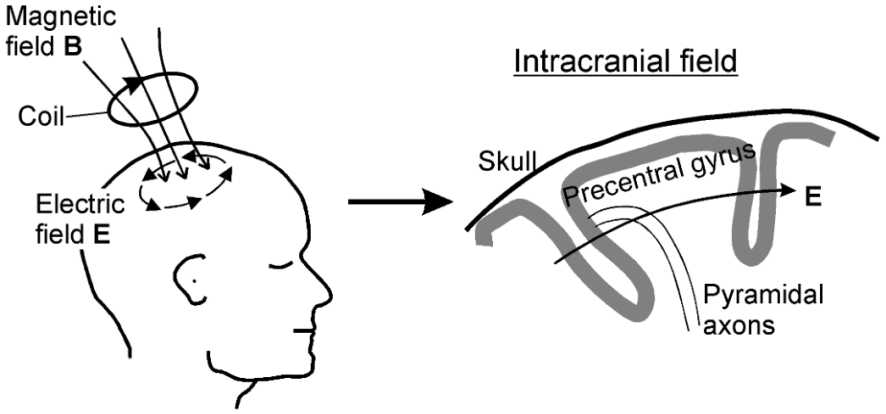

Figure 1.1: In TMS, an electromagnetic coil produces a magnetic field, which induces an electric field in the brain. This electric field causes membrane depolarization in the nerve cells that have a suitable orientation and position. If the membrane potential crosses the threshold voltage, an action potential is triggered [5]. Picture by Ruohonen [6].

Transcranial magnetic stimulation relies on changing magnetic fields. Sometimes static magnetic fields of permanent magnets are proposed for medical and therapeutic purposes. An example can be seen on the alternative medicine website *alive.com* [7], which describes several methods and treatments. These treatments are not recommended by the US National Institutes of Health [8]. There are suggested mechanisms how static magnetic fields could affect the human body, but so far there is no evidence that static magnets work better than placebo [9]. Changing magnetic fields, on the other hand, are known to affect the human body.

Traditionally, transcranial magnetic stimulation is conducted with an electromagnet, which is kept close to the subject's head. The electric current flowing in

the coil causes a magnetic field. When the electric current changes, the magnetic field also changes. The change in the magnetic field induces an electric field in the brain. This is illustrated in figure 1.1. The magnitude of the electric field, as well as the current produced by it, is proportional to the rate of change of the magnetic field:

$$E \sim \frac{\mathrm{d}B}{\mathrm{d}t}, \tag{1.1}$$

where E is the electric field, B is the magnetic field and t is time. The unit of electric field is V/m, volts per meter.

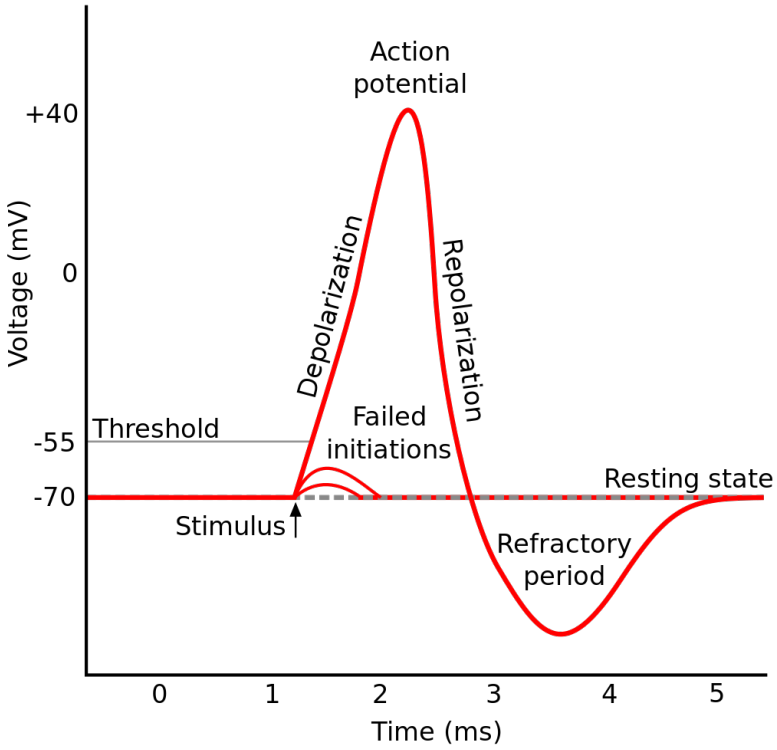

Figure 1.2: An action potential is triggered if the membrane potential rises above the threshold voltage. The action potential quickly depolarizes the membrane. The membrane potential then returns back to the resting potential. A new action potential can not be triggered before the refractory period has ended. Picture from Wikimedia Commons [10].

In transcranial magnetic stimulation, the rate of change of the magnetic field is more important than the absolute strength. An iron core would increase the rate of change and the strength, but would also become saturated in a strong magnetic field. The saturation magnetism would change the timecourse and the shape of the magnetic field, making the mathematics more complicated. Moreover, the weight of the iron increases the total weight of the coil, which makes it more difficult to hold the coil manually in place. Most TMS electromagnets have an air core [11]. The air core, as a term, also includes cores made of plastic and other non-magnetic materials.

The stimulation is delivered in very short magnetic pulses, which activate the nerve cells in the target area. The activation is based on the depolarization of the cell membranes. There are two important values of the membrane potential of a cell: the resting potential, which is the potential without an external electric field, and the threshold potential, at which an action potential triggers.

Figure 1.2 shows the timecourse of a typical action potential in a characteristic nerve cell. The resting potential of the cell membrane is -70 mV. If a stimulus manages to raise it to the -55 mV threshold, voltage-gated ion channels are opened in that part of the membrane. The ions move through the channels, increasing the potential quickly. The channels are deactivated after some amount of time, and the potential returns back to the resting potential. The next action potential can not be activated before the refractory time has passed [5].

In transcranial magnetic stimulation, the induced electric field changes the membrane potential of nerve cells. The exact effects depend on the orientation of the electric field relative to the nerve cell [6]. The nerve cells typically have long axons, which may be curved or twisted. Each axon is physically a part of one nerve cell, and can transmit information to one or more nerve cells [5].

If the threshold voltage is reached at one part of the axon, the action potential will travel to both directions. At the beginning of the axon, it stops and has no effect. At the end of the axon, it activates synapses, which excite (or inhibit) the next nerve cells. Often a single action potential is not enough to trigger an action potential in the next nerve cell [5]. Simultaneous excitation by multiple synapses is required. Therefore the pulse must activate a large amount of nerve cells to trigger brain activity in the area.

To increase the probability that many nerve cells are activated, the pulse should be strong. A strong electric field can activate an axon even when its orientation is not very favorable. In traditional TMS, the pulses are created by charging a capacitor and then unleashing the charge through the coil. The electric current is initially zero, but rises quickly to its maximum. The maximum value of the magnetic field is typically 1–2 teslas, and the pulses last a few hundred microseconds [11].

1.2 Disadvantages of present systems

Major disadvantages in the electromagnet-based TMS are noise and heat. The rapidly changing magnetic field exerts a force to the materials in the coil, causing an acoustic click up to 110–120 dB(A) [12]. This sound activates hearing-related brain areas simultaneously with the magnetic field that activates the target areas. In scientific experiments this can be countered by for example conducting control experiments with similar acoustic stimuli [13] or by auditory masking random noise via headphones. Coil heating is caused by the electric current. It limits the length of a TMS session and is sometimes countered by having a cooling system built in the coil [11].

In this study, a TMS system is built using permanent magnets. Our objective is to induce an electric field in the brain. The permanent magnets must be moved to achieve this. The system is tested by simulation and by measurements.

The new system would eliminate the noise and the heat problems. There would be no "coil clicks", because from the viewpoint of the magnet, the magnetic field is constant. The new system is not necessarily quiet. However, the acoustic noise from the machinery moving the magnet is continuous, so its effects are easy to eliminate from the data. The heating would be eliminated, because there is no electric current in the magnet. It is also possible that the new system would be cheaper to build than an electromagnet-based system.

As far as we know, there are no previous studies about moving permanent magnets to stimulate brain. In this study, we measure the fields induced by moving magnets. The results are used to find out whether practical TMS would be feasible with permanent magnets.

1.3 Desirable electric field strength for TMS

The advantages mean nothing if the new system is not capable to be used for transcranial magnetic stimulation. In this study, the stimulation is not applied on human or animal test subjects. It is therefore necessary to use earlier studies to define how strong a field is required.

This section focuses on the methods that are able to change the membrane potentials of the nerve cells so much that action potentials are triggered. There are some methods that can modify the brain activity in different ways, and they are addressed in the next section.

A typical electromagnet-based TMS coil would induce an electric field peaking at 200–250 V/m, when measured at a 15-mm distance from the coil surface. A typical pulse duration is 140–170 microseconds [14]. This induced electric field represents the maximum stimulator output, and is higher than what is required to stimulate brain activity.

One method to calculate the required electric field threshold is based on the reasoning that the cell membrane functions as a leaky capacitor. In electronic terms, a leaky capacitor can be modeled as an RC circuit. It is a circuit consisting of a charged capacitor and a resistor (see figure 1.4). A charged capacitor discharges through the resistor, and the charge eventually declines to zero. If an external current is constantly being fed to the capacitor, the charge in the capacitor eventually reaches a non-zero equilibrium value.

In case of a cell, an external electric field moves ions across the cell membrane, changing its potential. At the same time, ions are leaking back to the other side. Because of this, a membrane in a constant electric field eventually reaches an equilibrium potential. If the field is switched off, the membrane returns to its resting potential, which usually has a non-zero value.

Voltage V in an RC circuit follows differential equation

$$C\frac{\mathrm{d}V}{\mathrm{d}t} + \frac{V}{R} = 0, \tag{1.2}$$

solution of which is

$$V(t) = V_0\, e^{-t/RC}. \tag{1.3}$$

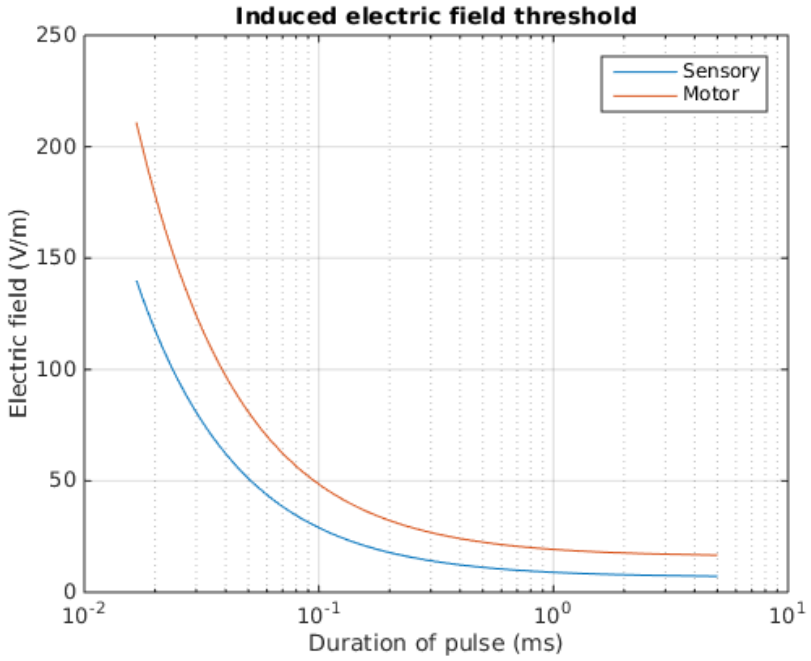

Figure 1.3: Neural stimulation threshold as a function of pulse duration. Duration means the time a pulse spends in the positive side, not the time between two peaks. Data by Bourland *et al.* [15]. As the duration of the pulse decreases, a stronger induced electric field is required to elicit a response.

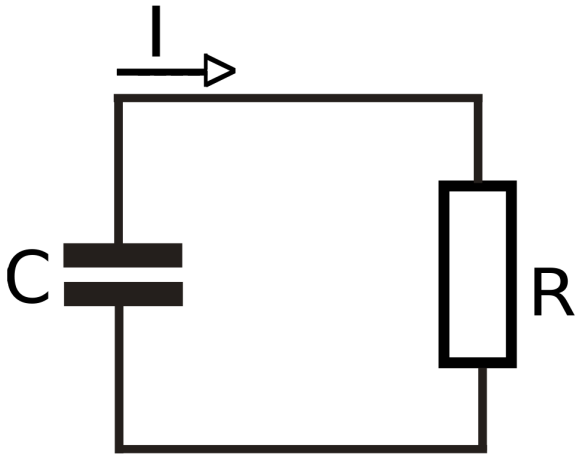

Figure 1.4: A charged capacitor discharges through the resistor, and the charge eventually goes to zero. This circuit is analogous to a cell membrane that has been charged by an external electric field. If the field is never shut down, the charge will not reach zero. Picture from Wikimedia Commons [16].

The charge of the capacitor

$$Q(t) = C \times V(t). \tag{1.4}$$

This means the charge of the capacitor in an RC circuit declines exponentially.

Another method to calculate the threshold is based on the research of the electrical stimulation. In there, the time average magnitude of the electric field required to cause stimulation of a peripheral nerve is given by the following relationship [17]:

$$E_{threshold} \equiv \frac{1}{T} \int_0^T E(t)\ \mathrm{d}t \geq E_r \cdot (1 + \frac{\tau_c}{T}), \tag{1.5}$$

where T is the duration of the pulse. This approximation characterizes the electric field with variables called rheobase (E_r) and chronaxie (τ_c). Rheobase is the lowest constant electric field that will trigger an action potential, and chronaxie is the time in which action potential will trigger if the field is twice as high as the rheobase [18].

If the strength of the electric field is lower than the rheobase, an action potential will never trigger, because the equilibrium potential is below the threshold voltage. If the strength is higher than the rheobase, the equilibrium potential is higher than the threshold voltage for triggering an action potential. The membrane potential changes gradually, and after enough time has passed, an action potential is triggered. The stronger the field is, the less time is needed before the action potential.

In the first method, the threshold declines as $\exp(-T)$, but in the second method the threshold declines as $1/T = \exp(-\ln T)$. Both are ideal models, and a real cell membrane is more complicated.

Values for rheobase and chronaxie are presented by Bourland *et al.* (original article [15], summarized in [11, ch. 5] and [17]). The resulting curves are in figure 1.3. Bourland stimulated the forearm, which was encircled with a solenoid coil and subjected to trapezoidal magnetic pulses. According to them, the rheobase values were 6.75 ± 2.06 V/m for a sensory response, and 16 ± 6.1 V/m for a motor response.

The values of chronaxie, according to the same study, are 329 ± 78.4 µs for a sensory response, and 203 ± 78.5 µs for a motor response [15]. More recently, Peterchev *et al.* [19] have estimated the chronaxie of the motor threshold to be 137 µs. They defined this using TMS on human motor cortex, which is closer to our research than the setup used by Bourland. According to Peterchev, there have been no TMS studies which estimate the rheobase.

Using the values of Bourland, the strength of a 1 millisecond long pulse should be at least 11.2 V/m for a sensory response, and 22.5 V/m for a motor response. If the duration was halved, the required values would be 11.6 V/m and 29.0 V/m, respectively.

When the induced electric field is stronger than the required threshold value, it only indicates that some kind of response will occur. It does not implicate that a stimulation with so weak field will have any practical use. One application for the new system could be therapy. Therapy sessions last a long time, 20–60 minutes, and heating of the coil becomes a problem during such session.

Smania *et al.* [20] used 20-Hz magnetic stimulation on human patients to treat the myofascial pain syndrome. The stimulation was targeted at the myofascial trigger point of the upper trapezius muscle. They spent 20 minutes per therapy session

and received results at mean stimulation intensity of $25 \pm 5.1\%$ from the maximum stimulator output, when using a figure-8-shaped coil. If the maximum stimulator output would induce an electric field of 200 V/m in brain, then a stimulator that induces 50 V/m in a similar setting would be sufficient for such therapy. The pulse duration is not reported by Smania. Nieminen *et al.* [14] measured a stimulator-coil combination that is similar to what Smania used, and its pulse duration was approximately 170 μs. If our pulse is longer, even lower field strength is required.

Other applications of TMS include mapping of brain areas, and treatment of depression [21]. It is likely that they need a field strength that is similar to the threshold value.

1.4 Applications for low-strength fields

Induced electric fields that are not strong enough to trigger action potentials in the nerve cells may still have some applications. One method, known as transcranial current stimulation (tCS), utilizes an electric current to induce an electric field. The other method uses a weak magnetic field for stimulation.

Some experiments indicate that the human brain will respond to weak magnetic fields as small as 0.1 mT [22–28]. Fields used in TMS are more than 10000 times higher. The frequency of the stimulation is an important factor. It seems the frequencies that are most likely to cause a response are around 60 Hz [22]. The mechanism by which low-strength magnetic fields can alter the brain activity is unknown. Marino *et al.* [22] reason that the mechanism probably does not involve direct alteration of the voltage-sensitive ion channels in the neuronal membrane.

This claim is supported by the work of Sonnier *et al.* [29], who measured the membrane potentials of human nerve cells that were subjected to an oscillating magnetic field for 5-second periods. The rate of change of magnetic field was 188.5 mT/s at its maximum. They detected no changes in the membrane potential, even though the system could have detected changes as small as 38 μV. They refer to earlier studies [23–28] which indicate such field strengths are sufficient to alter the electrical activity in animals and human subjects, and suggest these fields are detected by sensory cells.

Because the principles of this method are not well understood, it is unclear what its applications can be. Therefore it is not discussed further in this study. The rest of this section focuses on tCS.

In tCS, two electrodes are placed on the scalp of the subject. A typical placement is shown in figure 1.5. The current flows from the "active" electrode to the "reference" electrode, and induces an electric field along its path. The current can be either direct current (DC) or alternating current (AC). These have different effects. The amplitude of the induced electric field is in the order of 0.2–2 V/m [30].

An electric field of this magnitude does not directly induce action potentials [30]. However, it can change the firing rate of neurons, modulate their strength, or entrain the brain oscillations to the same frequency as the stimulation [30, 32]. The latter two processes are illustrated in figure 1.6. It can also cause long-term potentiation (an increase in synapse strength) and long-term depression (a decrease in synapse

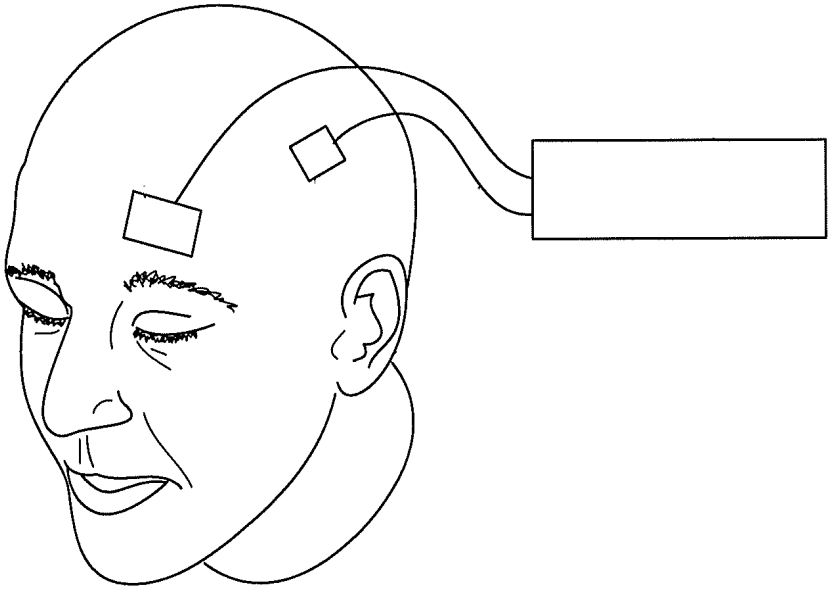

Figure 1.5: In transcranial current stimulation, an electric current flows between two electrodes. Typical area of an electrode is 25–35 cm^2 [30]. Picture by Bikson *et al.* [31].

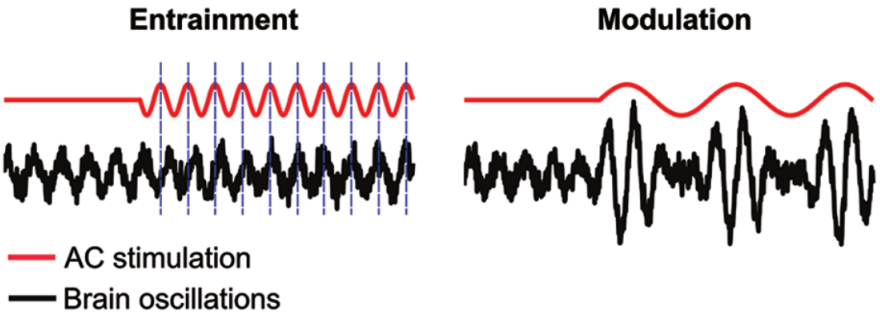

Figure 1.6: Alternating current tCS can entrain the brain oscillations by shifting their phase, or modulate their power at the stimulation frequency [32]. Picture by Reato *et al.* [32].

strength), which can last up to weeks and months [30].

Liebetanz *et al.* [33] found that direct-current-based tCS increases the velocity of cortical spreading depression. This suggests that such stimulation could be used as a treatment for pathologies that reduce cortical excitability, such as stroke, Parkinson's disease, and major depression [30]. Another suggested application of tCS is treatment of epilepsy [30].

In tCS, the stimulation is conducted continuously for 10–20 minutes [34]. Our system can not induce a constant electric field. Because the electric field changes over time, it would be equal to alternating current stimulation. Direct-current-based stimulation cannot be emulated with our system, which may rule out some potential applications.

Our system is based on a magnetic field. Magnetic field does not spread in the head like an electric current does. This means a system based on a magnetic field can achieve better focality than tCS.

In tCS, the current flows between two electrodes, and it is necessary to have some space between the electrodes, so that the current would reach the brain. Datta *et al.* [35] calculated that at 52-mm distance between the electrodes, 63% of the current reaches the brain and 37% flows in the scalp and the skull. Another factor that affects the focality is that the electrodes used for tCS are relatively large. Such electrodes distribute the current to a large area [30]. Large electrodes are preferred over small, because they produce lower current densities in the scalp and in the brain [30].

Most of the current that reaches the brain flows tangentially between the two electrodes. The "active" electrode is typically placed over the target area, and the other electrode is placed so that the effect of the current is thought to be minimal [30]. This means tCS always activates more than just the target area. With our system, this would not necessarily happen.

2 Mathematical methods

2.1 Calculating the induced electric field in the brain

Transcranial magnetic stimulation requires a changing magnetic field. To achieve this with a permanent magnet, the magnet must be moved.

For a point-like permanent magnet, the magnetic field $\mathbf{B}$ at point $\mathbf{r}_1$ can be obtained from

$$\mathbf{B} = \frac{\mu_0}{4\pi}\left(\frac{3\mathbf{a}\,(\mathbf{m}\cdot\mathbf{a})}{a^5} - \frac{\mathbf{m}}{a^3}\right), \qquad \mathbf{a} = \mathbf{r}_2 - \mathbf{r}_1, \tag{2.1}$$

where a is the distance between the point of observation $\mathbf{r}_1$ and the magnet location $\mathbf{r}_2$. A permanent magnet is defined by its magnetic moment $\mathbf{m}$, which points from the south pole to the north pole. Vector $\mathbf{a}$ points from the point of observation to the magnet.

The induced electric field can be calculated by the magnetic flux. The magnetic field passing through a surface A generates a magnetic flux

$$\Phi_A = \int_A \mathbf{B}\cdot \mathrm{d}\mathbf{A}. \tag{2.2}$$

Electric field $\mathbf{E}$ can be derived from the time derivative of the magnetic flux:

$$\oint_{\partial A} \mathbf{E}\cdot \mathrm{d}\mathbf{l} = -\frac{\mathrm{d}\Phi_A}{\mathrm{d}t}. \tag{2.3}$$

The calculations can be simplified with the spherical model. In the model, the head is approximated with a sphere. The spherical model assumes the conductivity in the head is spherically symmetric, *i.e.*, $\sigma(\mathbf{r}) = \sigma(r)$. When the model is used, the origin of the sphere should be based on the local curvature of the skull's inner surface [36].

What this assumption allows us to do, is approximating a single, tangential current element with a triangle [37]. The tip of the triangle is in the center of the assumed sphere. This is illustrated in figure 2.1.

A sphere with a radial primary current element produces no magnetic field outside. The same is true for a sphere with no current elements inside. A sphere with a tangential current element produces a magnetic field. If two radial current elements are added, they cancel the volume currents produced by the tangential element. The resulting triangle produces the same magnetic field as the original tangential current element [37]. Reciprocally, the electric field induced by an external coil can be obtained with the same triangle construction [14].

Assume the triangle is placed on the yz plane, with its center line along the z axis. The magnet moves along the x axis and its magnetic moment is along the x axis. In this geometry, the $\mathbf{B}$ field points to the x direction and the $\mathbf{E}$ field points to the y direction. Now that the direction is known, only the value of $\mathbf{E}$ needs to be calculated.

The triangle is defined as follows: height (length) is R, width of the base is h, and distance between the base and the origin is d. Thus the triangle's base is centered at point $(0, 0, d)$ and its tip is at point $(0, 0, d + R)$.

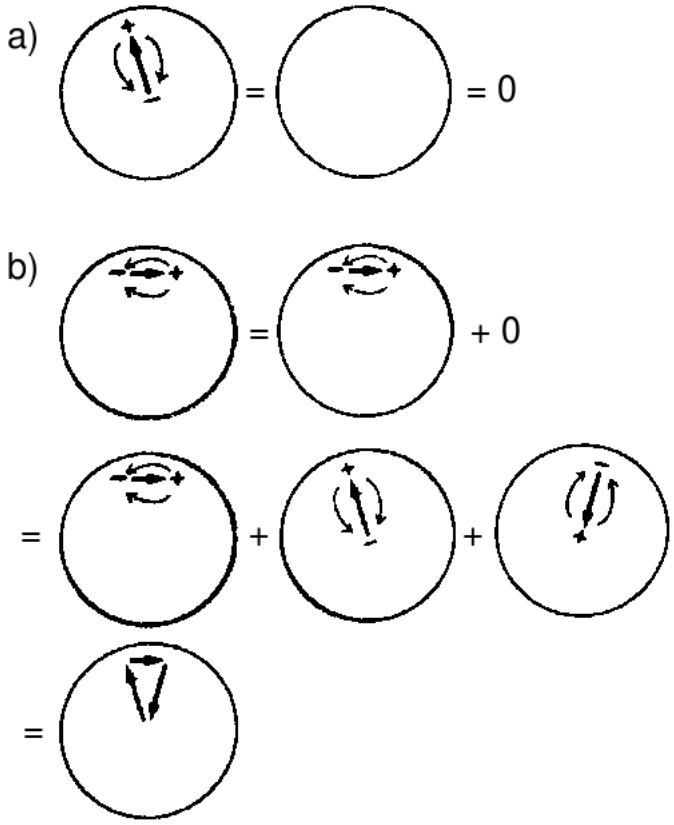

Figure 2.1: Formation of the triangle equivalent of a current dipole in the spherical model. a) A radial primary current element does not produce a magnetic field outside. b) If two radial source current elements are added to the tangential current element, the volume currents are canceled but the magnetic field remains unchanged. Picture by Ilmoniemi [37].

The magnetic flux through the triangle is

$$\Phi_A = \int_d^{d+R} \int_{-L(z)/2}^{L(z)/2} \mathbf{B}(y,z) \cdot \hat{\mathbf{e}}_x \, \mathrm{d}y \, \mathrm{d}z, \tag{2.4}$$

where $L(z) = (h/R)((R+d) - z)$ is the width of the triangle as the function of z. Note that $\mathbf{B}$ also depends on the x-coordinate and time, which at this point have been omitted for clarity.

For a very thin triangle, $\mathbf{B}$ can be approximated as $\mathbf{B}(y = 0)$. This allows us to calculate the y-dependent integral analytically. The magnetic flux takes the following form:

$$\Phi_A = \int_d^{d+R} (\mathbf{B}(z) \cdot \hat{\mathbf{e}}_x) \frac{h}{R} ((R+d) - z) \, \mathrm{d}z. \tag{2.5}$$

The integral of the electric field (equation 2.3) can be simplified with the spherical model:

$$\oint_{\partial A} \mathbf{E} \cdot \mathrm{d}\mathbf{l} = (\mathbf{E} \cdot \hat{\mathbf{e}}_y) \, h. \tag{2.6}$$

The final equation becomes

$$\mathbf{E} \cdot \hat{\mathbf{e}}_y = -\frac{1}{h} \frac{\mathrm{d}}{\mathrm{d}t} \int_d^{d+R} (\mathbf{B}(z,t) \cdot \hat{\mathbf{e}}_x) \frac{h}{R} ((R+d) - z) \, \mathrm{d}z, \tag{2.7}$$

where $\mathbf{B}$ is calculated according to equation 2.1. The induced electric field increases linearly with the velocity. It also increases linearly with the strength of the magnetic moment.

2.2 Measuring the induced electric field

Section 2.1 showed how the electric field induced by a permanent magnet can be calculated. Another way to obtain the induced electric field is to measure it. This can be done with a wire loop, in which a nearby moving magnet induces an electric current.

A magnetic field passing through a conductive loop (surface A) causes an electromotive force:

$$\mathcal{E} = \oint_{\partial A} \mathbf{E} \cdot \mathrm{d}\mathbf{l} = -\frac{\mathrm{d}\Phi_A}{\mathrm{d}t}, \tag{2.8}$$

where $\mathbf{E}$ is the induced electric field and Φ_A is the magnetic flux. The electromotive force can be measured directly with an oscilloscope. When all dimensions of the wire loop and the measurement setup are known, the electric field can be calculated.

The spherical model is used to simplify this integral. According to the spherical model, all radial currents are zero. This means a triangular wire loop can simulate a single, tangential current element inside a spherical conductor [37].

Dimensions of the triangle-shaped wire loop define dimensions of the brain. The sides of the triangle should be the same as the radius of the brain. The base of the triangle should be narrow, so that it can be used to approximate the electric field in one point.

In the spherical model, a radial current element in the brain produces volume currents, but does not alter the magnetic field that can be detected outside. A tangential current element also produces volume currents, but changes the magnetic field as well. In the triangle, there is one current element at each side. The radial current elements have the same length, so they cancel the volume currents induced by the tangential current element. This means the magnetic field induced by a triangle is the same as the magnetic field induced by a tangential current element alone [37].

In a practical measurement, the triangle must have some width, because a very small surface area results to a very small magnetic flux, and the signal is concealed by the noise. Another practical point is that the magnet is moved in such distance that the closest point is approximately 15–20 millimeters from the measurement coil. This emulates the skull and the scalp that would cover the brains of an actual test subject.

For a very thin triangle, the length of the sides is the same as the height. Let us consider a triangle with 10 mm width and 70 mm height. For such triangle, length of the sides are 70.18 mm. The triangle-shaped wire loop is considered a slice of a circle. This means its base should be curved. If the triangle is very thin, a flat base can approximate a curved surface. This would allow us to use 70 mm as the radius of the head, instead of actual 70.18 mm.

The triangle is positioned so that its tip is at the center of the head. The positioning of the triangle defines the direction of the coordinate axes used in that measurement. The triangle can only measure one component of the magnetic flux at a time. If the radial axis is considered the z axis, then the x and y components can be calculated by turning the triangle 90 degrees between the two measurements. The z component can not be measured with a triangle, but according to spherical model it should be zero (assuming the point of measurement is on the z axis).

In equation 2.8, the integral can be split to three parts; one part for each side of the triangle. Because radial electric fields are zero in the spherical model, the only part that remains is the electric field along the base of the triangle. The equation becomes

$$\mathcal{E} = \mathbf{E} \cdot \mathbf{d}, \tag{2.9}$$

where $\mathbf{d}$ is the base of the triangle in a vector form. The maximum of the electric field component is equal to the maximum of the electromotive force divided by the width of the triangle.

2.3 Measuring the magnetic moment of a magnet

Calculating the induced electric field requires knowledge of the magnetic moment. For a non-rotating permanent magnet, the magnetic moment $\mathbf{m}$ is constant over time. The magnetic moment can be estimated by measuring the force between two magnets. The force can be calculated with the Gilbert model, which models each magnet as two magnetic charges near its poles. This model is valid when the distance between the magnets is large compared to their sizes.

In case of two identical cylindrical magnets with radius q and height h, at a distance of x from each other, the force between the magnets is [38]

$$F_M = \left(\frac{B_0^2 \, (\pi q)^2 \, (q^2 + h^2)}{\pi \mu_0 h^2} \right) \left(\frac{1}{x^2} + \frac{1}{(x+2h)^2} - \frac{2}{(x+h)^2} \right). \tag{2.10}$$

B_0 is the magnetic flux density at the immediate vicinity of the magnet:

$$B_0 = \frac{\mu_0 M}{2}. \tag{2.11}$$

Magnetization of the magnet is

$$M = \pm \sqrt{\frac{4\pi \, F_M \, h^4}{\mu_0 \, (q^2 + h^2) \left(\frac{1}{x^2} + \frac{1}{(x+2h)^2} - \frac{2}{(x+h)^2} \right)}}, \tag{2.12}$$

where all required quantities can be measured from a physical magnet.

In case of a cubic magnet, the radius can be replaced with the equivalent spherical radius (the side length multiplied by $\sqrt{4/\pi}$), which keeps the volume of the magnet unchanged.

To find out how the shape of the magnet affects the electric field, the magnet can be divided to several small sections, which are modeled as individual magnetic moments. If the magnet is made of uniform magnetic material, its magnetization is constant in all sections of the magnet. This means if all sections have the same volume, the magnetic moment of one section is the total magnetic moment divided by the number of sections.

The magnetic moment of one section comes from the definition of the magnetization:

$$\mathbf{M} = (N/V) \, \mathbf{m}, \tag{2.13}$$

where V is the volume of the magnet and N is the amount of magnetic dipoles in the magnet.

3 Verification of calculations with drop tests

The simplest way to move a magnet at a constant speed, in a repeatable manner, is dropping it. To ensure it would drop in a straight line down, the magnet was dropped through a 2 m long plastic tube. The induced electric field was estimated with a triangle-shaped coil. The coil was placed outside the tube, near its bottom end, so that the magnet would have time to speed up. Even though the magnet was accelerating because of the gravity, its speed could be approximated to be constant during a short time interval.

The drop tests were replicated with simulations done in Mathematica. Comparison of the experimental and the computational data would tell us how accurate our calculations are. The mathematics required for the simulations are explained in the previous chapter.

3.1 Tools

3.1.1 Magnets and their magnetic moments

Magnets used in the drop tests were cylindrical rare-earth magnets with 10 mm radius and 10 mm height. There were no documents about the magnetic moment, so it was measured. The measured quantity was the force exerted by a magnet. A magnet can lift up magnetic objects when the magnetic force is greater than the force of gravity. At the equilibrium position,

$$m_M\, g = F_M, \tag{3.1}$$

where F_M is the force between the magnets (equation 2.10), m_M is the mass of a magnet and g is the gravitational acceleration (9.819 m/s^2 at Helsinki, Finland).

One magnet was placed inside a thin, transparent plastic tube. A second magnet was held above it, and when the distance was small enough, the magnet inside the tube would stick to the ceiling. The distance was then increased until the magnet would drop from the ceiling.

The distance was measured with a plastic ruler at accuracy of 1 mm. At 57 mm distance, the magnet would visibly begin to dislodge from the ceiling, but would not yet drop. At 58 mm, the magnet would drop. The equilibrium position was thus at the distance of 57 ± 1 mm.

The mass of the magnet was measured with an electronic balance. The magnet was measured on top of a 91 mm tall styrofoam piece, and the balance was zeroed when the magnet was held approximately 5 mm above the piece. At this distance, the influence of the magnetic force was smaller than the variation between the weighing results. The final result was 23.05 ± 0.02 grams.

Using equation 2.12, the magnetic moment was estimated to be 1.91 ± 0.06 Am^2. The magnetization of the magnet was $(61 \pm 2) \times 10^4$ A/m.

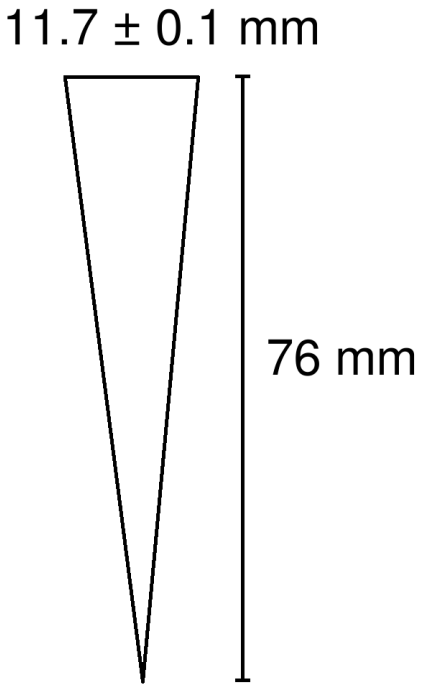

Figure 3.1: A triangle-shaped coil was used for measuring the induced electric field. At the tip, the wire was not wound tight so that it would approximately follow the outline of a 76-mm tall triangle. Such winding is somewhat imprecise, but it should not cause much difference in the resulting electromotive force, because the distance from the magnet is so large at the tip.

3.1.2 Triangular measurement coil

The induced electric field was estimated with a triangle-shaped coil. The coil was built around a triangle-shaped plastic block, and consisted of a single wire loop. The block was manufactured with a milling cutter. Target dimensions of the triangle were 10 mm width and 70 mm height. Due to the limitations of the manufacturing method, these dimensions differ somewhat.

The width of the base was estimated to be 11.7 ± 0.1 mm. The height was 71.4 ± 0.1 mm. The error comes from the uncertainty of the manufacturing method. The diameter of the electric wire was 0.3 mm, so it is not reasonable to measure any other dimensions in a greater degree. The tip of the triangle was dull, with width of approximately one millimeter. Ideally it should have been perfectly sharp, but attempting to mill a perfectly sharp edge with available tools would have splintered the triangle.

If the triangle was the same size as the target dimensions, the angle between the base and a side should be 85.91 degrees. If the angle was precisely correct, the height of the triangle would be 81.7 mm, if it was not dull. The angle was measured to be 85.6 degrees, which would result to a 75.8 mm long triangle. In calculations, 76 mm was used as the height of the triangle and the radius of the head.

3.2 Methods

3.2.1 First series: m points down

The first series of drop tests were conducted so that the magnetic moment vector was directed along the tube's axis. As illustrated in figure 3.2, we placed a round magnet in a round tube. Therefore this was the only position in which we could trust the magnetic moment vector would keep its direction during the fall.

The cross-section of the tube was a circle with diameter approximately 22 mm. The magnet was a cylinder with 20 mm diameter, so it would fit to the tube if it was dropped flat side down. In that case its magnetic moment vector would point either up or down. The radius of the magnet was increased by rolling several layers of tape around the magnet. If the radius was too small, the magnet would turn around during the fall. If the radius was too high, the magnet would be randomly slowed down by the friction, and the variance in speed would be large between individual drops.

The magnet was placed on the top end of the tube, and it would accelerate because of gravity. It would be slowed down by the air resistance, so its velocity had to be measured. The tube would increase the air resistance to some extent. The main purpose of the tube was to control that the magnet falls in a straight line and does not turn around during the fall.

The speed of the magnet was measured with two circular coils along the tube. When the magnet would pass through a coil, it would induce a voltage. The voltage measured from those coils would show two peaks, one for each coil. The velocity of the magnet is the distance of two coils divided by the time between the peaks.

With practical drop heights (below 2 m), the magnet will not reach a constant speed. However, its speed is approximately constant when observing a short period of time.

Dimensions of the coils were: radius 50 ± 0.1 mm, height 4.0 ± 0.1 mm, distance between two coils 109 ± 1 mm. The triangular coil had equal distance to both circular coils.

3.2.2 Second series: m points to the side

The second series of drop tests were conducted so that the magnetic moment vector points to the side, while the magnet was moving down. In this position, the shape of the electric field should be different than in the earlier series.

A major challenge in this setting is that the tube has a cylindrical cross-section, which allows the magnet to rotate around the tube's axis. If the magnetic moment vector points down, this is not a problem, because it will point down even after the rotation. Now that the magnet has been tipped 90 degrees, the rotation around the tube's axis must be prevented to ensure the magnetic moment always points to the same direction.

Padding was attached to the magnet so that it would not rotate perpendicular

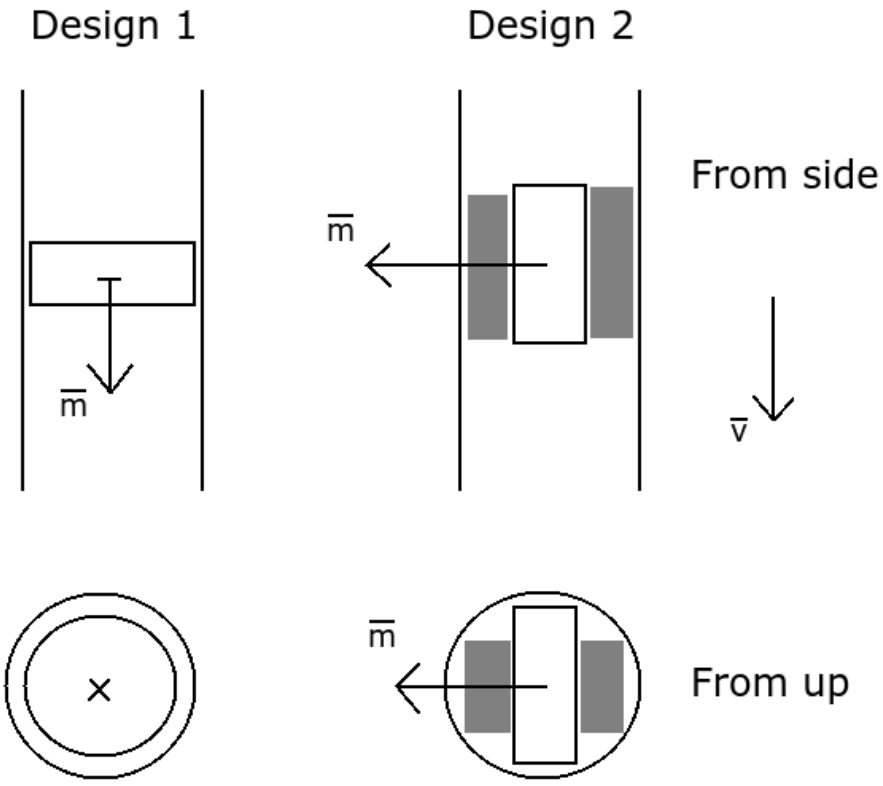

Figure 3.2: The magnet was turned 90 degrees by attaching padding to it. In the first design, it does not matter if the magnet rotates around the tube's axis; the direction of the magnetic moment stays unchanged. In the second design, such rotation would change the direction of the magnetic moment.

to the tube's axis. That is, the magnetic moment would stay pointed to the side and not turn up or down. However, this could not prevent rotation around the tube's axis. Preventing such rotation would require a tube with a quadrilateral cross-section. Another challenge is that if the orientation of the magnet is done manually before each drop test, there will be some variation in its direction. Orientation of the magnet is illustrated in figure 3.2.

The drop tests were averaged to decrease the effect of the noise. The shape of the result should be correct, but the absolute values of the signal should decrease because of the variation in the orientation. These errors should be taken into account when interpreting the final results. If the variation is normally distributed around the desired orientation, with the standard deviation of 5 degrees, the peak would decrease by 0.38%. The peak would decrease 5% if the standard deviation was 18.5 degrees.

3.3 Results

3.3.1 First series

A permanent magnet was dropped through a plastic tube, and it would accelerate because of gravity. The induced electric field was measured with a triangular wire loop. The magnet had a magnetic moment of 1.91 ± 0.06 Am^2, which was measured in section 3.1.1. In the first series of the drop tests, the magnetic moment vector points down and the magnet drops down.

The drop tests were monitored with an oscilloscope. The speed of the magnet was measured with two circular coils at the distance of 109 ± 1 mm from each other. They were connected in parallel, and the voltage over the whole circuit was monitored with an oscilloscope. Two peaks would be shown, one for each coil. The velocity of the magnet could be calculated by dividing the distance travelled by the time spent.

The average velocity was first calculated between all 111 drop tests. Then only those drop tests at the distance of $\pm 1/2$ standard deviations from the average were selected. This formed a new data set of 48 tests. The measured voltage for that data set is shown in figures 3.3 and 3.4.

The time between the peaks was 20.75 ± 0.11 ms. The error is the standard deviation of the individual drop tests. The average velocity was 5.25 ± 0.08 m/s.

The magnet fit the tube very tightly. The radius of both the tube and the magnet (covered with several layers of tape) were measured to be 21.9 ± 0.1 mm. This indicates the magnet did not have space to turn around, and its magnetic moment vector should point to the same direction during the fall. Velocity should be the only thing to change between each individual drop. There was little variation in the velocity between individual drop tests, which indicates the air resistance and the friction were similar in each drop.

The strength of the induced electric field was measured with a triangle-shaped coil. It was estimated by the electromotive force, the voltage caused by the passing magnetic flux. The results from the triangular coil are shown in figure 3.4. The

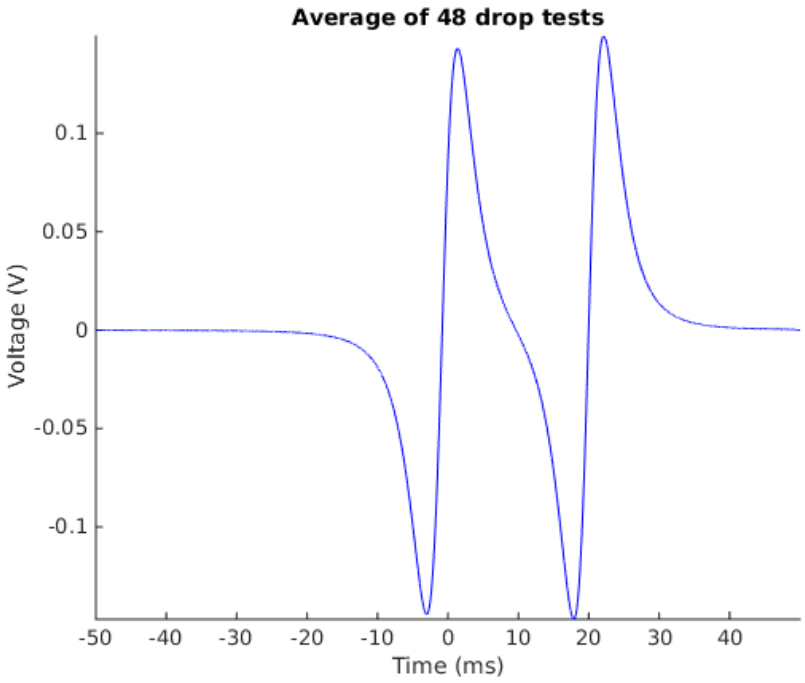

Figure 3.3: Two circular coils were attached to the same channel. The channel shows two peaks where the magnet falls through the coils. The time difference between the two peaks can be used to estimate magnet's velocity.

magnet passes the triangle between approximately −10 and +20 ms. Because the magnet had a similar velocity in all drop tests, the peaks should be in the same place in each measurement. If there is variation, the height of the peaks should decrease and the pulse duration should increase. The velocity results indicate that this variation was less than 2%.

The data set was averaged to reduce noise. The peak height of the voltage (0.274 mV) was calculated from the averaged data. Individual drop tests had some variation in the voltages. The standard deviation of the individual results was used as the uncertainty of the averaged result. The final peak height was 0.27 ± 0.02 mV.

In the measurement geometry, the triangle is laid on the yz plane and the magnet moves along the x axis. The magnetic moment vector is also along the x axis. Therefore the triangle measures the y component of the electric field, E_y. It has the same shape as the electromotive force in figure 3.4. Component E_x is zero.

The maximum of E_y was obtained with equation 2.9. The width of the triangle was 11.7 ± 0.1 mm. Therefore the maximum was 0.023 ± 0.002 V/m. The uncertainty of the result is 8.7%.

3.3.2 Second series

In the second series of the drop tests, the equipment stays otherwise same, but the magnetic moment vector points to the side. The triangular coil was turned 90 degrees around its axis so that it would stay perpendicular to the magnetic field lines. In the measurement geometry, the triangle is now laid on the xz plane and the magnetic moment points to the $-y$ direction. The measured component is therefore E_x. Results are shown in figure 3.5.

The velocity was measured with the same coils as in the first series. Their position relative to the magnet is different, so the strength of the signal is decreased. However, there are still two clearly visible peaks.

A smaller data set was selected from all drop tests, using same method as in the first series. This data set used 54 drop tests out of the original 159. The time difference was 19.611 ± 0.048 ms. The velocity of the magnet was 5.56 ± 0.06 m/s. This is larger than in the first series, because the air resistance is smaller.

The data set was averaged and the peak height of the voltage was calculated. The result was 0.092 ± 0.015 mV. Equivalent E_x is 0.0079 ± 0.0013 V/m. The uncertainty of result is 16.5%.

The variance in the results is much larger than in the first series. One possible cause is the orientation of the magnet. It is unknown how the magnet rotates during the fall and how large the rotations are, but its shape definitely allows some rotation to happen.

The peak voltage is lower than in the first series. If the magnet was pointlike, it should not matter which to direction it is moving. In the actual measurement, there are two factors which may decrease the voltage. The first factor is the increased distance from the magnet's surface, and the other factor is the shape of the magnet.

In the first series, the distance between the magnet's surface and the tube's inner surface is less than 1 mm. In the second series, the cylindrical magnet is dropped

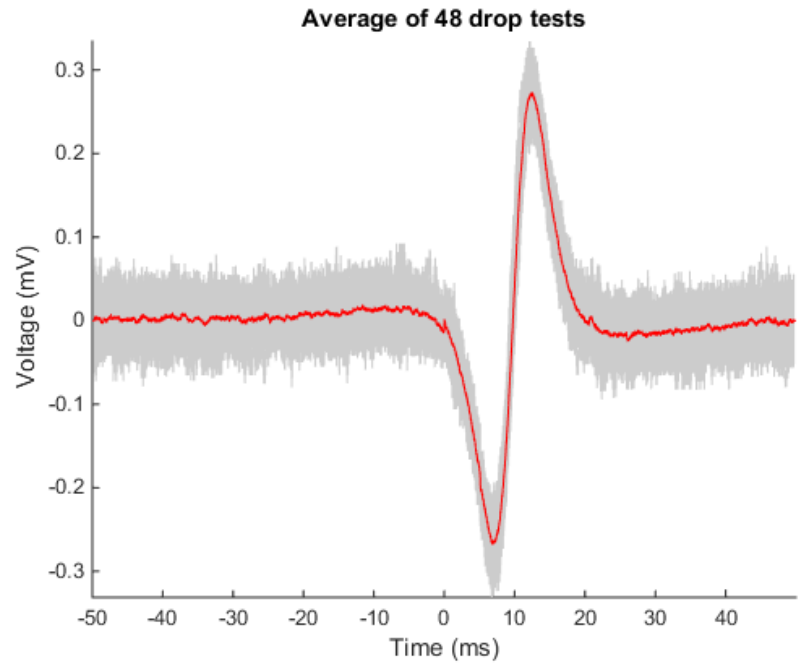

Figure 3.4: First series. Results from the individual drop tests (shown in grey) were averaged. The averaged result (shown in red) has a very clear shape. This figure represents the electromotive force, but the electric field component E_y has the same shape.

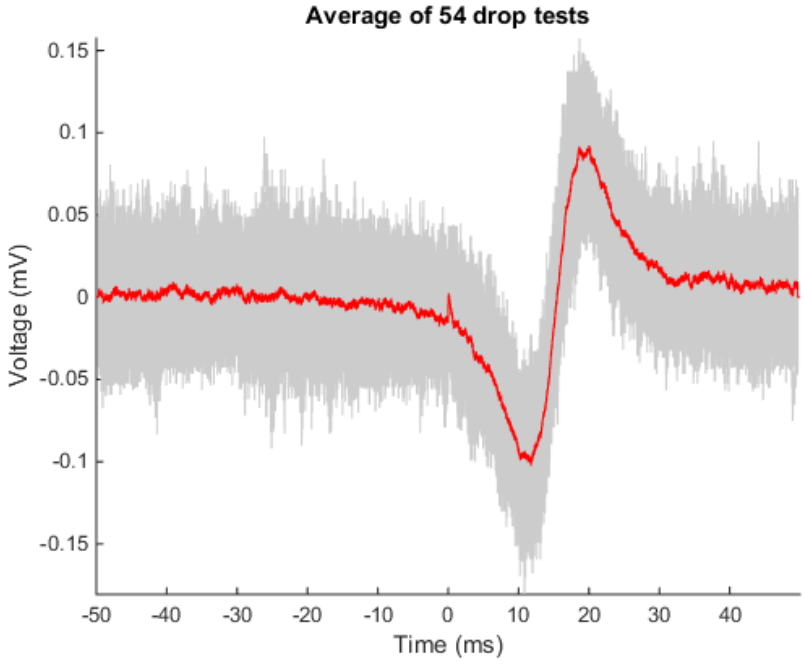

Figure 3.5: Second series. The voltage decreases 50% compared to the first series. This may be explained by the increased distance from the magnet's surface, and the shape of the magnet.

on its side, so when it passes a certain point in the tube, the perpendicular distance to the magnet's surface is initially 11 mm as the bottom edge passes the point of observation. The distance decreases to 1–2 mm at the middle of the magnet, and then increases back to 11 mm at the top edge. This means that in the second series, the magnetic field has more time to rise to its maximum, and it rises more slowly.

3.4 Comparison of measurements and calculations

Both series of drop tests were simulated in Mathematica. The method is explained in section 2.1. The calculations were done with equation 2.7, in which the magnetic flux density was calculated with equation 2.1.

The velocities and the geometrical dimensions are the same as in the previous section. The only variable that was used in the simulations, but not in the previous section, is the strength of the magnetic moment (1.91 ± 0.06 Am^2). It was estimated in section 3.1.1.

To take the shape of the magnet into account, the magnet was modeled as multiple magnetic moments. This was done by cutting the magnet to $2 \times 2 \times 1$ millimeter blocks (thinnest in the z direction), and then calculating if the center of a piece was inside the magnet or not. There were 800 pieces in a magnet. Each piece had a magnetic moment of $m/800$, so that the total magnetic moment would not change.

The results are shown in figures 3.6 and 3.7. It seems the simulation and the measurement are in the same range. In the first series, the simulated peak is 27% higher than the measured peak, and the simulated peak is narrower. In the second series, the simulation is 4% higher than the measurement. If this difference between the accuracy of the two simulations was caused entirely by the uncertainty in the orientation, it would require that the standard deviation of the angle was 36.57 degrees (assuming the angle was normally distributed around the desired orientation). It is very likely that the variation in the angle was not this big.

Averaging can decrease the height of peaks, because they occur at different points of time in each drop test. This point depends on the velocity of each individual drop test. The error caused by averaging was decreased by only using drop tests that had velocity within $\pm 1/2$ standard deviations from the mean.

The remaining differences between the simulations and the measurements are most likely caused by errors in the magnetic moment, or errors in the distance between the magnet and the measurement coil.

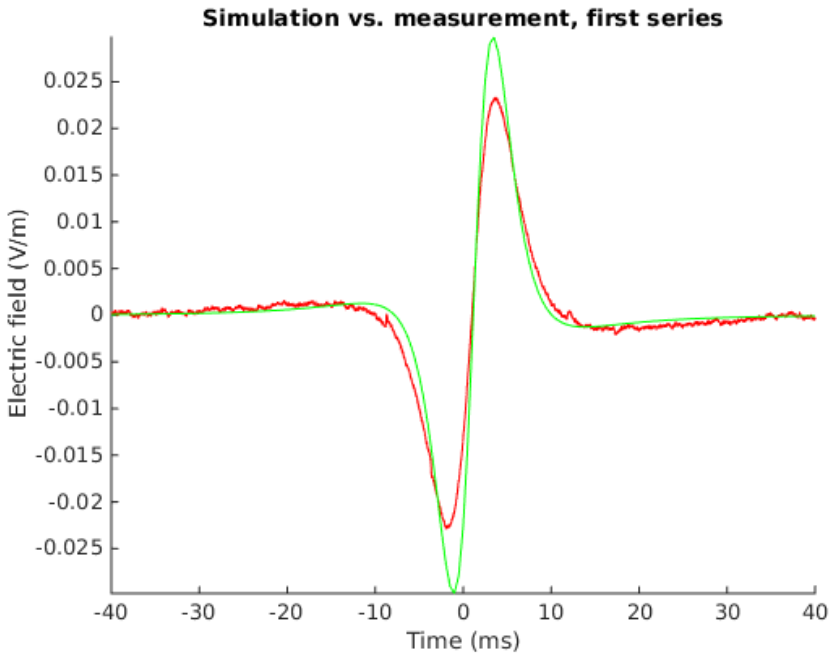

Figure 3.6: Drop tests in which the **m** points down. The measured E_y is shown in red and the simulated result is shown in green.

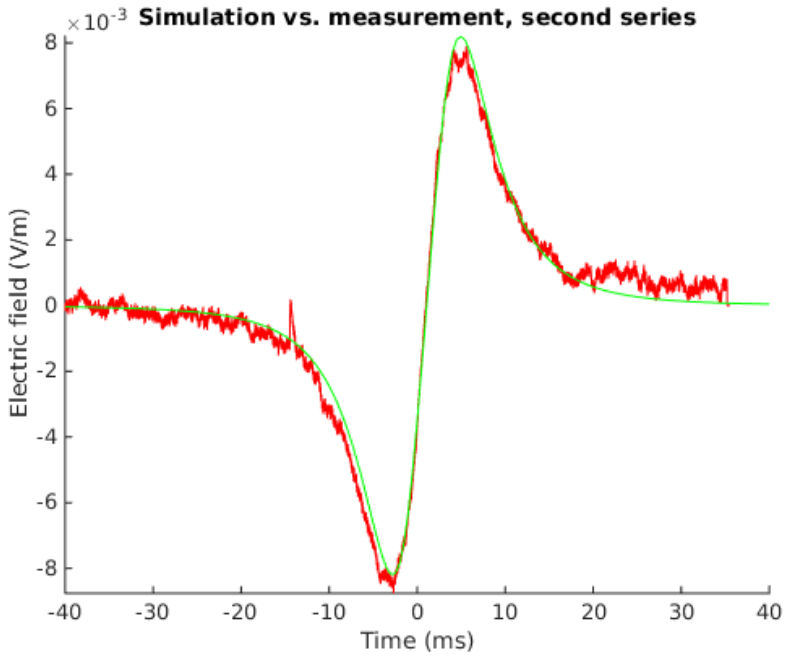

Figure 3.7: Drop tests in which the **m** points to the side. The measured E_x is shown in red and the simulated result is shown in green.

4 A prototype with stronger electric field

Stronger magnets and a faster movement speed are the most practical methods to increase the induced electric field. Several magnets were attached together to increase the total magnetic field. To achieve faster movement speed, magnets were attached to a wheel. A wheel can achieve higher velocities than what we could achieve by dropping the magnets. In the drop tests, the limitation is the space, *i.e.*, how high can we drop the magnet from. In the rotation tests, the limitation is the strength of the structure, *i.e.*, how high centrifugal force it can safely withstand. A rotating magnet would also allow us to repeat the magnetic pulse at regular intervals.

4.1 Magnets and their magnetic moments

The magnets used for building the prototype were cubic rare-earth magnets with 20 mm side length. According to the documents, the strength of the magnetic material is grade N52. All magnets were identical.

The grade of a magnet represents its maximum energy product, which can be calculated as the area of the largest rectangle that fits under its normal demagnetization curve [39]. This number does not depend on the magnet's volume. For a grade N52 magnet, the maximum energy product is equal to 4.1×10^8 J/m^3.

The magnetic moment was measured as previously in section 3.1.1. The equilibrium position was reached at the distance of 72.5 ± 1 mm. The mass of a magnet was 51.9 ± 0.1 g, according to documents.

Using equation 2.12, the magnetic moment was estimated to be 6.59 ± 0.15 Am^2. The magnetic moment was calculated with an equation designed for cylindrical magnets. The shape of the magnet was corrected for by using the equivalent spherical radius 10 mm $\times \sqrt{4/\pi} = 11.28$ mm.

The poles of the magnets were located by bringing two magnets close to each other, separated by a wooden block, and watching how the magnets would orient themselves. All magnets were compared to the same magnet. It was not necessary to know whether the marked pole was the north or the south. This would have been easy to check with a compass.

4.2 Comparison of some possible magnet layouts

The layout of the magnets was selected so that the strongest peak in the electric field would be maximal. This was best achieved by first introducing magnets that had north (or south) pole down, and then introducing magnets that had the opposite pole down. When such boundary would pass the point of measurement, there would be a large peak in the electric field. What matters is the absolute height of each peak, not the difference from a negative peak to a positive peak. 32 magnets were used to create the pattern.

In the calculations, the magnet was rotating on a circular track with 1 meter radius at frequency of 10 revolutions per second (600 per minute). The orbital velocity was 62.9 m/s. The rotation happened in the xy plane, and the triangle

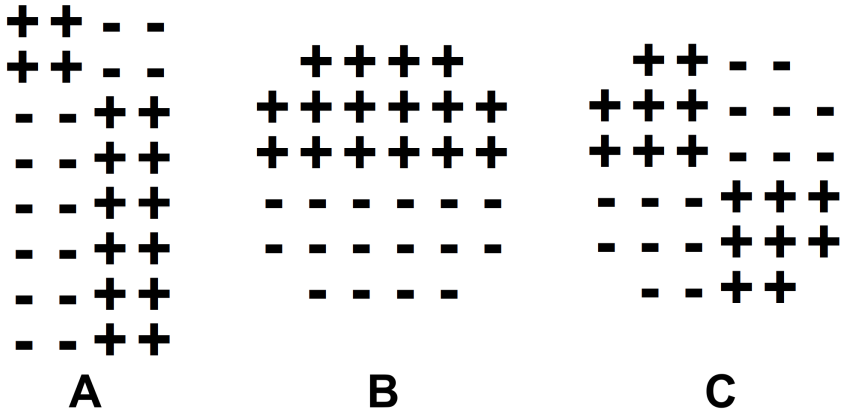

Figure 4.1: Three most promising layouts for the magnet placement. In terms of this image, the magnets would be moving in a straight line down, so the point of measurement would move across it from the bottom to the top.

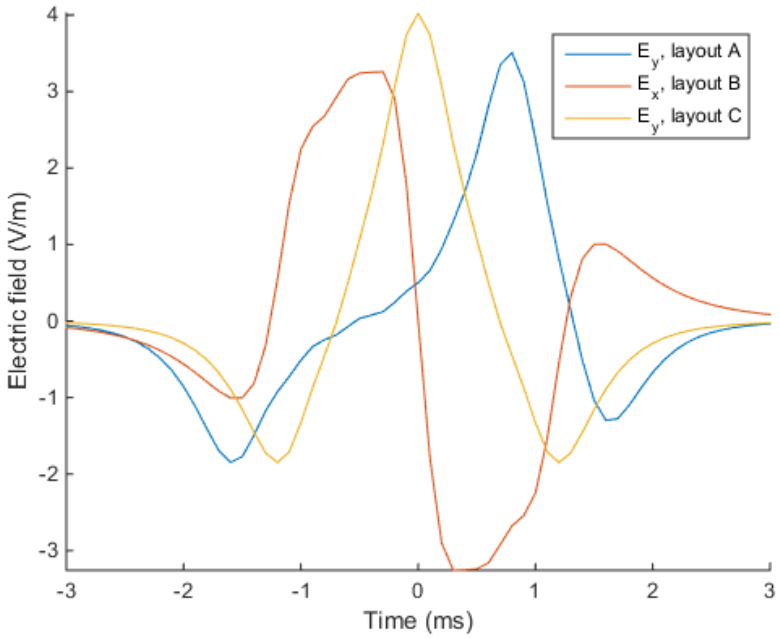

Figure 4.2: E_y or E_x calculated for the layouts A, B, and C. Out of these layouts, layout C has the highest peak.

was along the z axis. The base of the triangle was at 20 mm distance from the magnets' surface. Each magnet was split to $10 \times 10 \times 1$ mm blocks (thinnest in z direction). This accuracy seemed good enough for comparing these layouts. There were 80 blocks per magnet, 2560 in total. Each millisecond was split to 10 time points. On a desktop computer, the calculation time was 35 minutes.

The three most promising layouts are presented in figure 4.1. Their electric fields are presented in figure 4.2. These diagrams represent the x or y component of the electric field only. The other components were calculated with smaller amount of blocks and time points, and they seemed to be in the order of 10% of the strongest component.

In layout A, the first 6 rows of magnets are identical, so that the situation would stabilize after the first peak. Then the second peak would have a higher impact to the charges moving across a cell membrane. In layout C, the first 4 rows were moved closer to the center, one extra row in the each side, so that the change of the magnetic field in the center of the disk would be even higher. This resulted to a higher peak in the electric field. In layout B, the change of the magnetic field is higher, as indicated by the peak-to-peak difference, but the absolute height of the peak is smaller. The layout C was used in the final prototype.

The magnets were held in place with a plastic grid, which had holes for each magnet. There was 5 mm of plastic between each magnet. Ideally there would have been nothing between individual magnets, but because of the magnets' strength, such grid would have been very difficult to build. A 20-mm thick iron sheet was placed on the magnets, to channel magnetic flux back to the other side. The magnets were covered with a 3-mm aluminium sheet from the other side. Aluminium should not affect the magnetic flux in any way.

If the magnetic flux was perfectly channeled through the iron sheet, the energy density on the other side would double. The energy density is proportional to the square of the magnetic flux density B, and B is proportional to the magnetic moment m. If the channeling was perfect, the magnetic moment of each magnet would effectively be multiplied by $\sqrt{2}$. This multiplier should be the absolute theoretical maximum, so the actual multiplier would be between 1 and $\sqrt{2}$. In the calculations of this section, the iron sheet was not taken into account.

4.3 Moving the magnet

The magnet block was built from 32 magnets, a plastic grid, an aluminium sheet, and an iron sheet. The block was attached to a lathe (Stankoimport model 1M65-5, number 2789, manufactured in the Soviet Union). The lathe had a rotating disk with 1 m diameter and a potential rotation speed up to 500 revolutions per minute. The total weight of the magnet block was approximately 8 kg, mostly because of the iron sheet. The block is shown in figure 4.4.

The magnet block was attached to an iron bar and a counterweight, which brought the total weight to almost 50 kg. The iron bar was bolted to the wheel to hold it in place during the rotation. The block was placed so that its center was travelling at a track with 80 cm diameter (40 cm radius). The orbital velocity was

thus 20.9 m/s. The final setting is shown in figure 4.5.

The magnet block was rotated so that the magnetic moments were parallel to the wheel's axis. The wheel's axis was parallel to the ground. The measurement device was placed in front of the wheel.

The measurement device was first introduced by Nieminen *et al.* [14, 40]. It consists of two triangular wire loops, built perpendicular to each other. It could simultaneously measure both tangential components of the induced electric field at a certain point. This point could be selected with two servo motors that were attached to the triangle to move it. The triangles had 70 mm height and 5 mm width. The measurement device is shown in figure 4.3.

The measurement device was connected to a data-acquisition unit (NI DAQPad-6015, National Instruments), which was connected to a laptop. A LabView program was used to control the measurements.

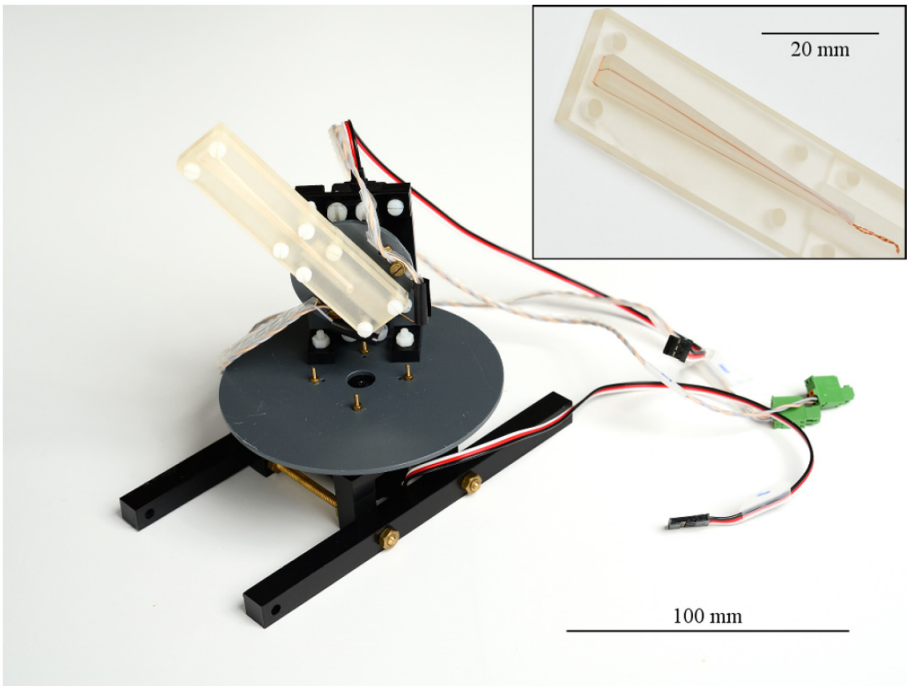

Figure 4.3: The measurement device. The two triangular coils can be rotated with two servo motors. The first motor is attached to the white plastic block and the second motor is under the round disk. Picture by Nieminen *et al.* [14].

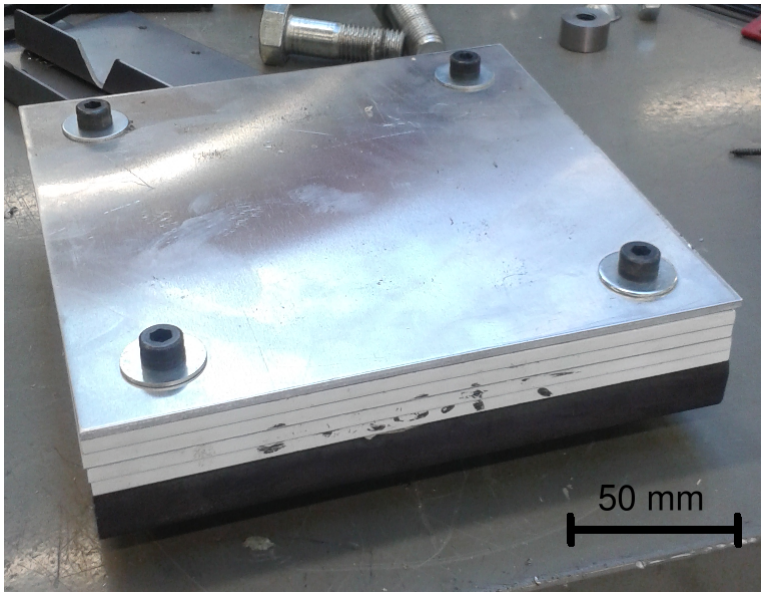

Figure 4.4: The magnet block. Magnets are held in place by a plastic grid, and covered by an aluminium sheet from the top.

Figure 4.5: The magnet block was attached to a lathe. In the picture, the magnet block is on the left and the counter weight is on the right. Both are attached to an iron bar. The rotational radius of the block's center is 40 cm.

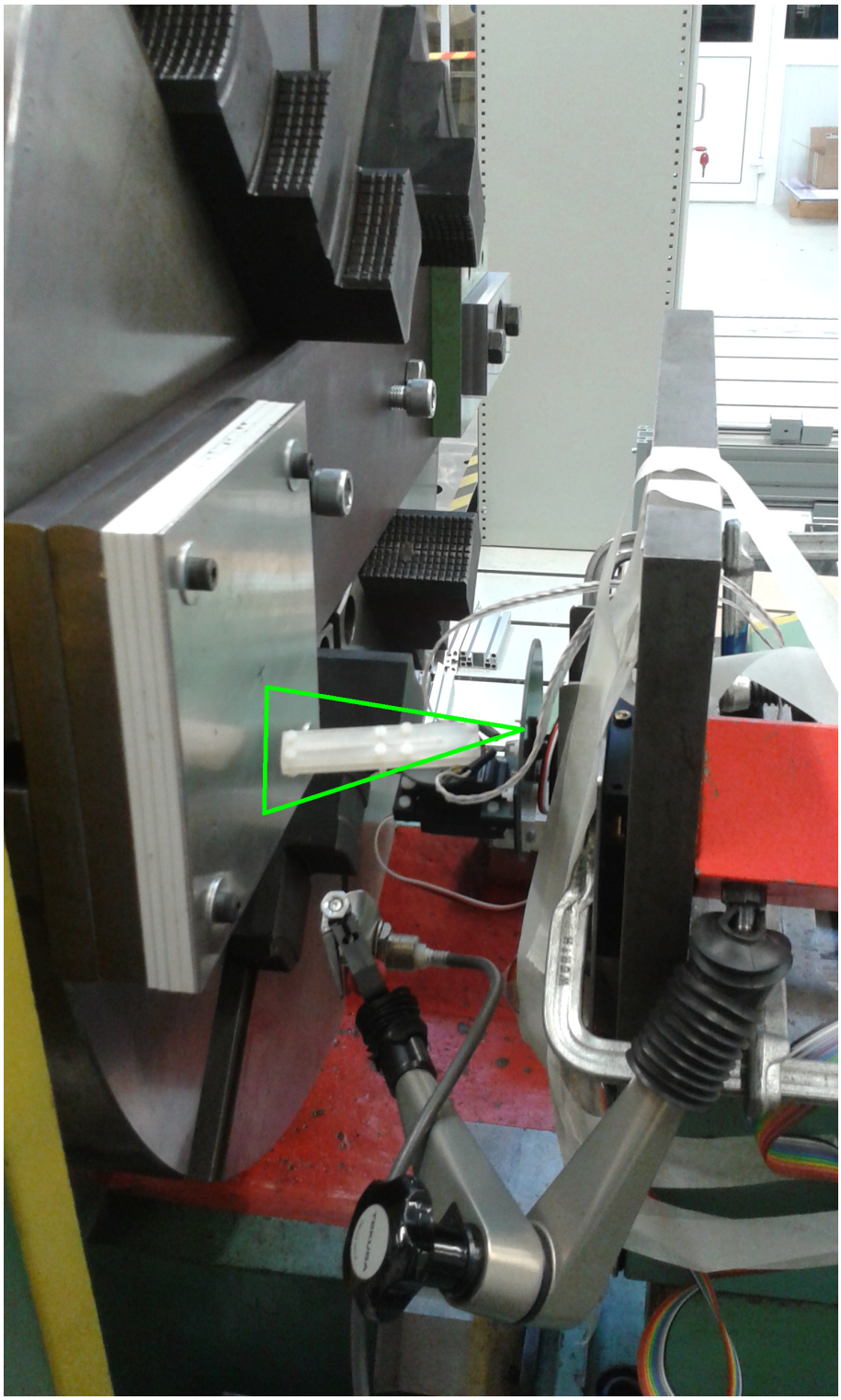

Figure 4.6: The measurement device in the final setting. The green triangle marks the triangular coils, which are protected by the white plastic case.

4.4 Results

The magnet block was rotated on a circular track, and the induced electric field was measured with a triangular coil. The voltage in the coil was sampled at a frequency of 50 kHz. To find out the rotation rate of the system, some measurements were conducted with a lower sampling rate, which offered a longer time window without increasing the amount of the samples. The electric field was first measured at the center position of the coil, at many different distances between the coil and the magnet. This was used to calculate the attenuation as the function of the distance.

The measurement coil was placed in the center position (perpendicular to the magnets' surface). The induced electric field was measured at 16.3–30.3 mm between the measurement coil and the magnets' surface. The distance splits to the following parts: 0.3 mm between the magnets and the aluminium plate, 3.0 mm aluminium plate, 11–25 mm air, and 2.0 mm plastic covering the coil. The highest value of the electric field at each distance was used for the further calculations.

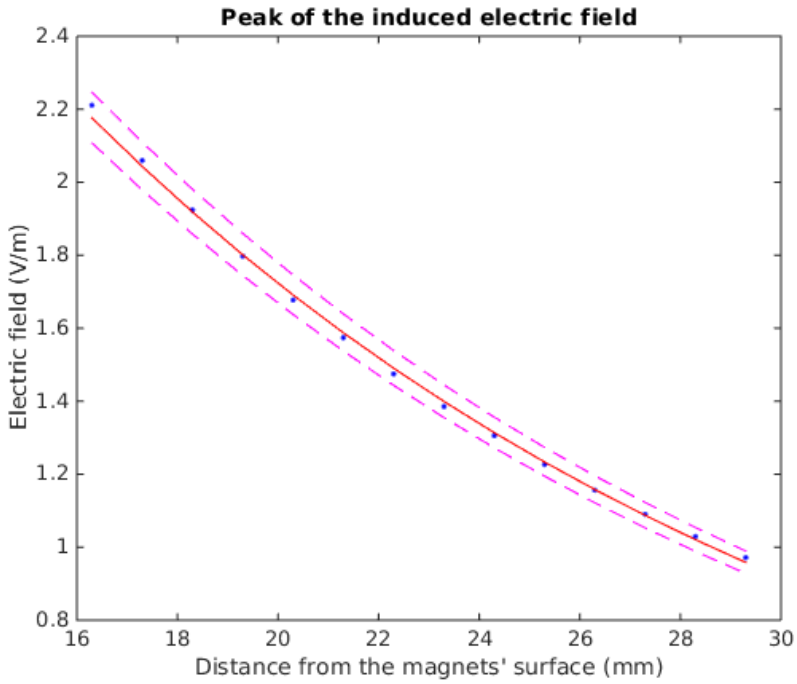

Figure 4.7: The strongest point of the induced electric field as the function of distance from the magnet. The exponential fit is shown in red and the error curves are shown in magenta. Absolute values of the peaks are used here; the highest peaks were negative due to the placement of the magnets.

The height of the peak as function of the distance are shown in figure 4.7. It shows that the induced electric field gets stronger, when the coil is moved closer to the magnet. Figure 4.8 shows one pass of the magnet as function of time.

The function $\beta \exp(\alpha\, z)$ was fitted to the data. The coefficients were $\alpha = -63.1/\mathrm{m}$ and $\beta = 6.086$ V/m. The coefficient of determination $R^2 = 0.9987$.

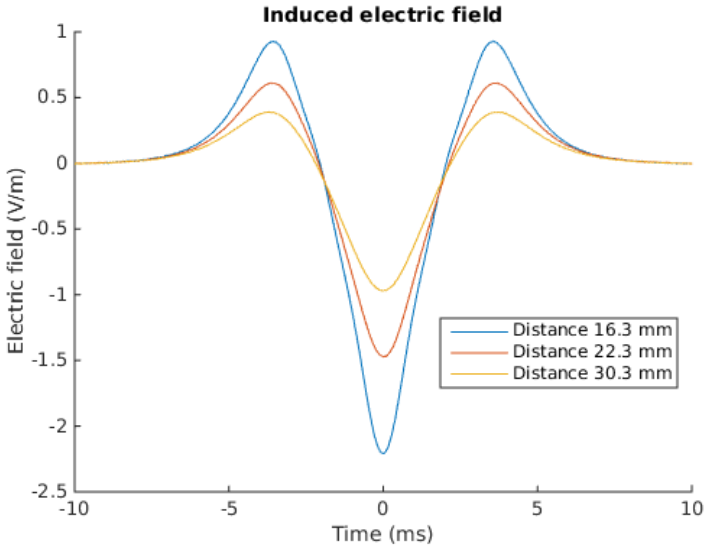

Figure 4.8: The waveform of the induced electric field, when the coil is in the center position. At the center position, the peak value of the electric field should be higher than in any other position. The peak was 2.17 V/m high at the 16.3 mm distance.

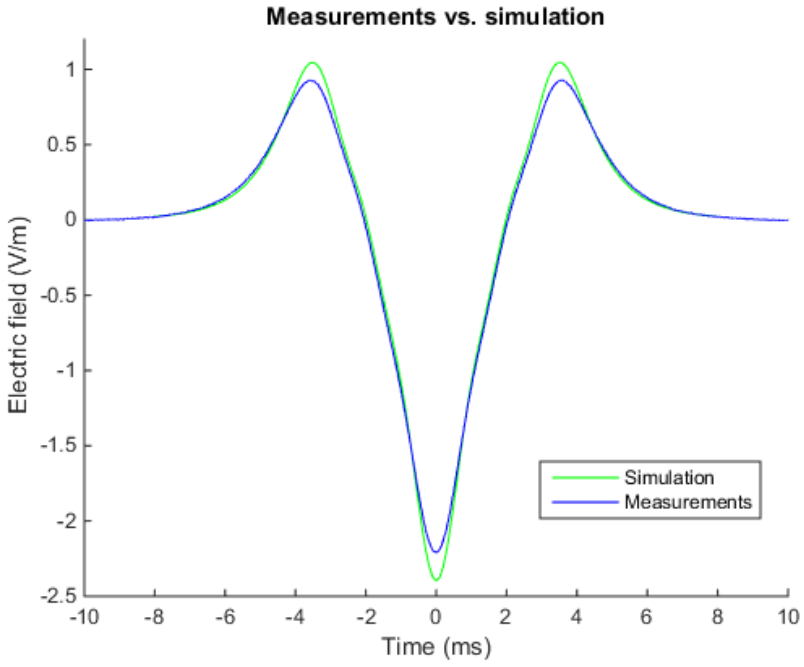

Figure 4.9: Comparison of the simulation and the measurements, at the 16.3 mm distance. The simulated peak is 8.4% higher than the measured one.

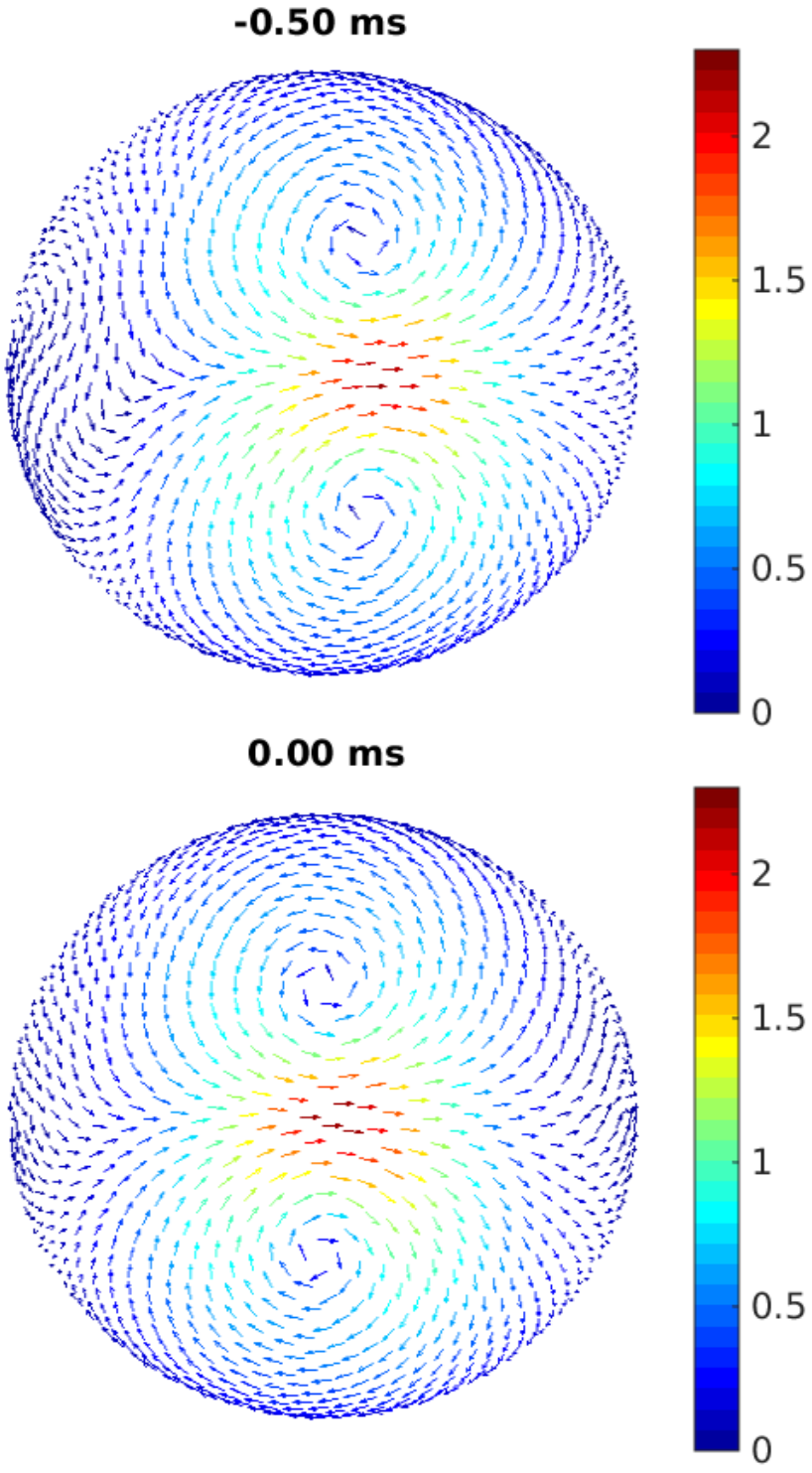

Figure 4.10: Direction and strength of the induced electric field at time points 0 ms and -0.50 ms, measured at the distance of 16.3 mm. At 0 ms, the center of the magnet block is directly next to the center of the measurement device. Each picture represents vectors on the surface of a half-sphere, shown from above. The center position of the measurement coil is at the center of each picture.

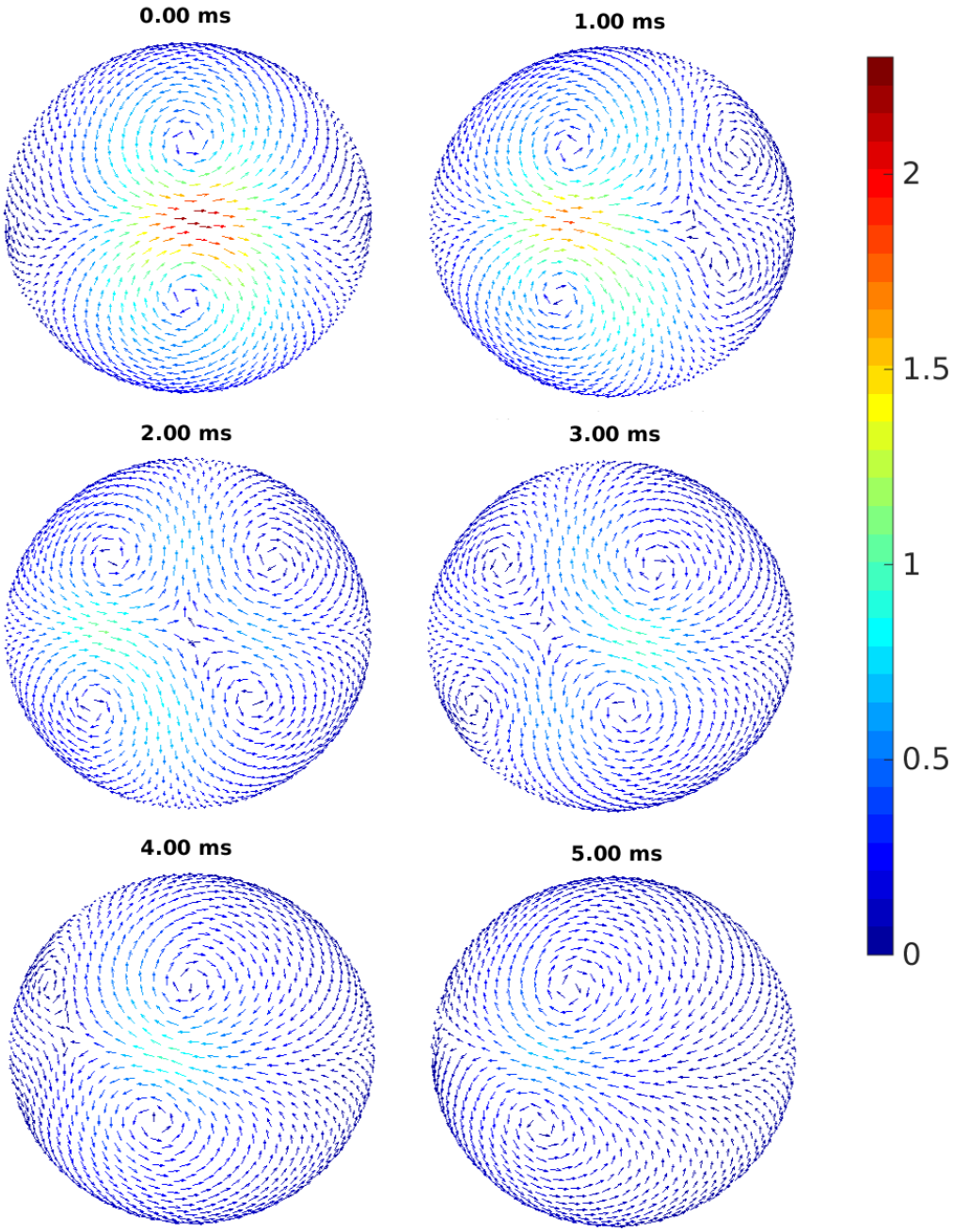

Figure 4.11: Direction and strength of the induced electric field from 0 ms to 5.00 ms, pictured at 1.00 ms intervals. At 0 ms, the magnet block's center is the closest to the center position, and the electric field there is at its maximum. At 1.00 ms, the field has decreased and the has maximum moved to the left, but the direction still stays the same. At 2.00 ms, the point of measurement is closer to the edge of the block than to the center. The field is changing its direction, and its value at the center point is zero. Between 3.00 and 4.00 ms the point of measurement has passed the edge of the block. The field has turned 180 degrees and reaches a local maximum at that point. After the edge has passed, the field eventually declines to zero.

At 20 mm distance, the peak of the induced electric field was 1.72 ± 0.06 V/m. At 16.3 mm distance, the peak was 2.17 ± 0.07 V/m. The error was calculated from the norm of the residuals of the polynomial fit (0.0320), which was placed into an exponential function. No error was defined for the original measurement results.

The pulse duration was 4.1 ms at the 16.3 mm distance. There was a slight increase in the duration as the distance was increased. At 30.3 mm distance the duration was 4.4 ms. This can be seen in figure 4.8. There is some variation in the rotation rate during the measurement, but it is not large enough to explain these differences.

The measurements were also compared to the calculations. The iron was expected to increase the electric field, because it would channel the magnetic flux back from the other side. If the channeling was perfect, the electric field would have been multiplied by $\sqrt{2}$ (a 41% increase). A simulation calculated this way had 8.4% higher peak than our measurement. This is shown in figure 4.9. This result does not contradict the $\sqrt{2}$ multiplier. The difference is so small that it can be explained by other uncertainties in the simulation.

The electric field was examined more thoroughly at the distance of 16.3 mm. The field was measured in 1000 different positions at the surface of a half-sphere. These measurements were used to find out the direction of the electric field.

The rotation rate was measured separately at each point. This was done by sampling a separate measurement with a lower sampling rate, so that two pulses would fit into one sample. The time between those pulses would tell us the rotation rate. The actual data were measured after that measurement, during another rotation of the wheel. The knowledge of the rotation rate was used to normalize each data to the mean rotation rate.

The rotation rate was set to 500 revolutions per minute, but the actual rotation rate was 507.49 rpm on average. This is equal to 8.46 revolutions per second. All measured rotation rates were within $\pm 0.2\%$ from the mean.

Figure 4.10 shows the direction of the electric field. It indicates that the magnet and the coil were aligned quite accurately; the magnet moves directly to the left (in terms of the picture), and the largest field vector points directly to the right. This justifies the fact that earlier we used only one component of the field to calculate the peak. At the maximum, the other component should be zero.

The magnet layout was planned so that the electric field distribution would be similar to the distribution of a figure-8-coil (shown in figure 4.12). Our results support this. It can be seen that the field forms two "circles", and the electric field is strongest at the intersection of those circles. Ideally those circles should be placed symmetrically, so that their centers would be at the same vertical axis when the time is 0 ms. Our measurement results seem to follow this model.

Figure 4.11 can be used to estimate the focality of the stimulation. The stimulation activates the brain areas in which the electric field increases above the threshold. The maximum of the field should be above the threshold, and the stimulation causes activation in a broader area. Nieminen *et al.* [14] measured various TMS stimulators and defined their focality based on the area where the induced electric field is over $1/\sqrt{2} \approx 71\%$ of its maximum. For a typical figure-8-coil, the activated area was

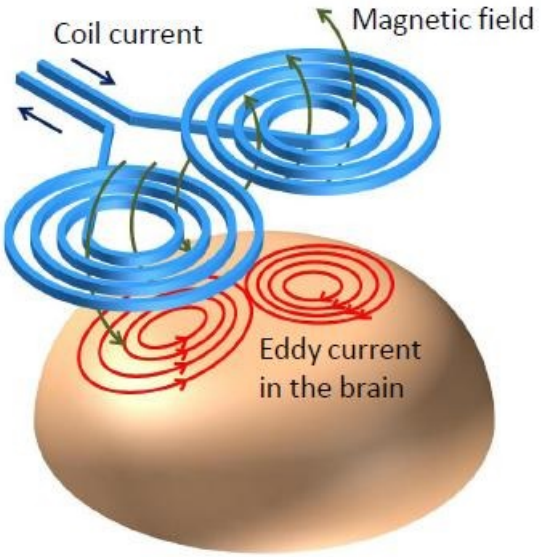

Figure 4.12: A figure-8-coil induces an electric field that is strongest below the intersection of two circular coils and weaker below the center of each circular coil. The electric field in the brain has the same direction as the induced eddy currents, which flow to the direction opposite to the rate of change of the currents in the coil [41]. Picture by Sekino *et al.* [42].

approximately 3×5 cm.

If we estimate where our field is above 1.5 V/m (70% of the maximum), the activated area would be an ellipse with 5 cm width and 3 cm height. This means our system and a typical TMS system have similar focality. At this accuracy, the estimation can be derived from figure 4.10; the diameter of the circle is 14 cm.

However, in our system the maximum of the field moves at least 7 cm on the surface of the brain before it drops below 1.5 V/m. This is different from what would happen with an electromagnetic TMS coil, location of which is kept static. Most likely this is not a problem in the actual brain stimulation, but it requires the patient is positioned very carefully to prevent activation of unwanted brain areas.

4.5 Suggested improvements for the future

The electric field induced by our prototype is not strong enough to trigger action potentials in human nerve cells. For a final product, the field should be at least ten times higher. The electric field increases linearly with the magnet's velocity. The velocity can be increased by increasing the radius and the rotational frequency. Other methods to increase the electric field are acquiring stronger magnetic material, bringing the magnet as close to the head as possible, and modifying the magnet layout.

4.5.1 Velocity

The velocity depends on the radius r and the rotational frequency f as follows:

$$v = 2\pi f r. \tag{4.1}$$

In our tests, the radius was 40 cm. This is a place for improvement. It is reasonable to estimate that a wheel with a radius of 150 cm could be used. With a protective casing, the machine would need a 4×4 meter space in the horizontal plane. This is similar to the space used by an MRI machine. Such wheel could be supported by laying it on supporting wheels, like the turntable in a microwave oven. Increasing the radius to 1.5 meters would increase the peak of the electric field by 275%.

The rotational frequency could also be increased. The things that increase with it are the centrifugal force, acoustic noise, air resistance, and the air flow around the wheel. A higher frequency also requires a stronger motor. The air resistance and the air flow could be removed by placing the wheel in a vacuum. It would increase the distance between the magnet and the test subject, so even stronger field would be required for stimulation.

Centrifugal force is defined as

$$F = \frac{m\,v^2}{r} = 4\pi^2\, m r f^2, \tag{4.2}$$

where m is the rotating mass. An 8-kilogram magnet rotating at a radius of 1.5 meters, with rotation rate of 84 revolutions per second (10 times faster than in our tests), would inflict a centrifugal force of 3.3×10^6 N on the machine. If the magnet is held in place by a 20×2 cm steel bar, the bar should have a tensile strength of 825 MPa to not to deform. A common steel is not strong enough for this, but maraging steel alloys have yield strength up to 2600 MPa [43].

This indicates it would be possible to build a system with much higher rotational frequency than what we used. If the frequency is multiplied by ten, the peak of the induced electric field can also be multiplied by ten.

In our measurements, the pulse duration was approximately 4 ms. Increasing the frequency tenfold would reduce the duration to 400 µs. According to figure 1.3, this would increase the threshold required for neural stimulation. The threshold can be approached mathematically by the convolution of the electric field and the decay function.

In mathematics, the convolution of a continuous function f and a continuous function g is defined as

$$(f * g)(t) = \int_{-\infty}^{\infty} f(t-s)\, g(s)\, \mathrm{d}s. \tag{4.3}$$

For discrete functions, such as our Mathematica results, this can also be calculated as a sum:

$$(f * g)(n) = \sum_{k=-\infty}^{\infty} f(n-k)\, g(k). \tag{4.4}$$

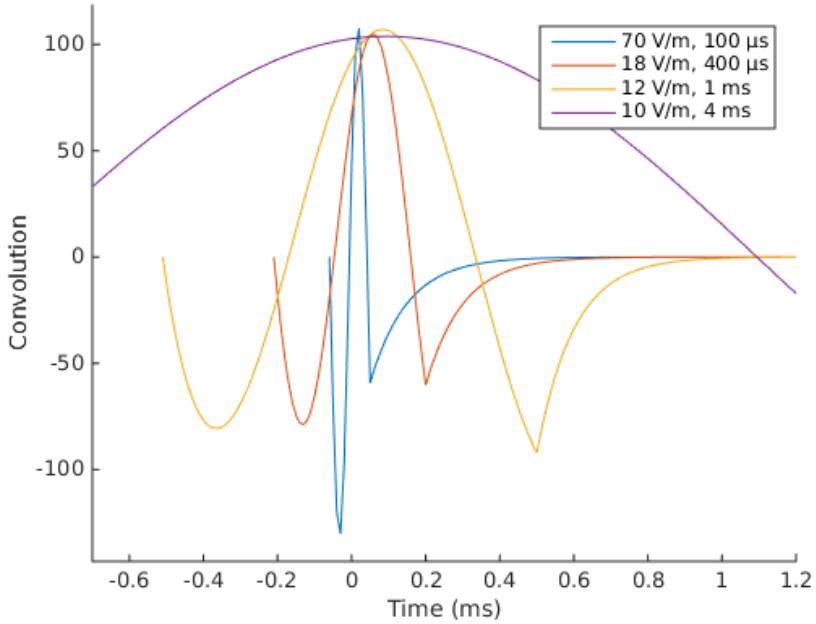

Figure 4.13: Convolutions of several different pulses with an exponential decay function. Zero values have been removed to keep the diagrams clean. The time constant is 300 µs. The diagrams show that a short pulse must be stronger to achieve the same effect as a long pulse.

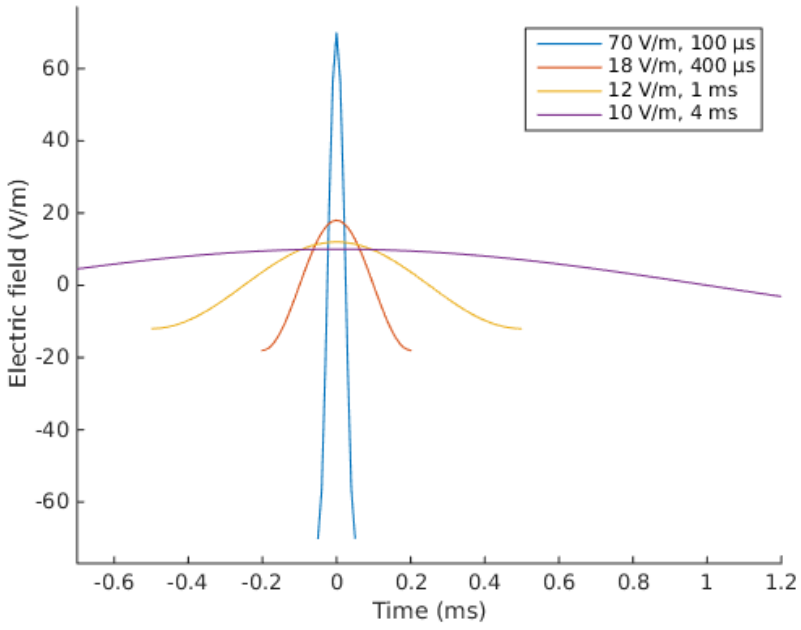

Figure 4.14: The same pulses before convolution. All pulses have the same shape: a cosine function from $-3\pi/2$ to $3\pi/2$ near the origin, and zero elsewhere. This shape has been adjusted for the desired pulse duration.

The decay function comes from the RC circuit model. Voltage V in an RC circuit was solved in section 1.3:

$$V(t) = V_0\, e^{-t/\tau}. \tag{4.5}$$

This time we define a time constant $\tau = RC$. The textbook by Malmivuo and Plonsey [44] reports that the time constant of a nerve cell membrane is in the order of 150–300 µs. A more accurate value has been measured by Peterchev *et al.* [19], who estimated it to be 200 ± 33 µs.

The values of convolution represent the membrane potential over time, but the values are relative and can only be compared within one picture. The electric field does not affect the membrane potential of every cell in the same way, because that depends on the physical dimensions and the alignment of the cell. Axons of the nerve cells have variable length, and they can be bent or twisted.

Figure 4.13 shows the influence of the pulse duration, when the time constant $\tau = 300$ µs. The original pulses are shown in figure 4.14. As the duration of the pulse decreases from 4 ms to 400 µs, the required electric field increases by 80%. This shows that increasing the velocity is advantageous; the electric field increases more than the threshold does.

4.5.2 Other factors

The magnet layout in the system was selected according to calculations in section 4.2. The selection criterion was the maximum of the peak in the electric field. Other points that should be considered are the shape and the duration of the pulse. In section 1, we mentioned a relationship between the strength and the duration of an electric field. This relationship was derived from one experimental study, but it can be tested for various time constants using convolution.

The convolution was calculated for the layouts A, B, and C, using time constants 100 µs and 300 µs. As previously, each magnet was split to $10 \times 10 \times 1$ mm blocks, the radius of rotation was 1 m, the rotation frequency was 10/second, and the iron was not taken into account. Each millisecond was split to 40 time points. These results are shown in figures 4.15 and 4.16.

Out of these layouts, it seems that the layout we used for the tests was the best. The layout A would become better than the layout C, if the time constant was large enough, because the pulse is longer than the others. However, this did not yet happen with the time constant 300 µs, and the actual time constants of the nerve cells are lower than that.

There is room for improvement in the distance between the magnets. If the magnets were placed closer to each other, the field would increase. When assembling the magnet block by hand, this is not possible, because the force required for pushing a magnet to its place is large even with 5 millimeter distance. With industrial machinery, it should be possible to assemble a magnet system with less than 5 mm between the magnets. By our calculations, the increase achieved with 0 mm distance between the magnets is 25%.

The strength of the magnetic material was grade N52. The next possible grade would be N54. With today's technology, N54 cannot be reliably produced in large

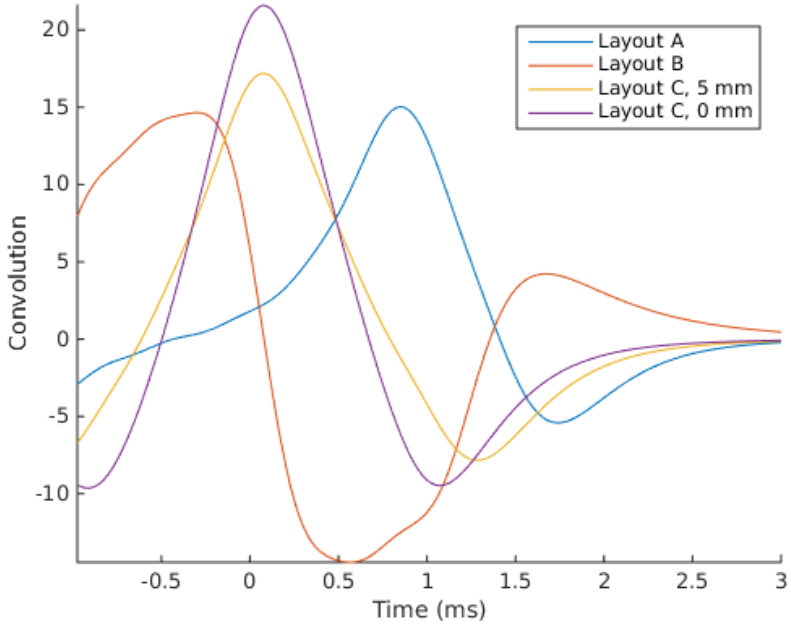

Figure 4.15: Convolution of the electric fields and the exponential decay function. Time constant $\tau = 100$ µs. Out of these layouts, layout C is clearly the best. For comparison, the layout C is also shown with 0 mm distance between the magnets.

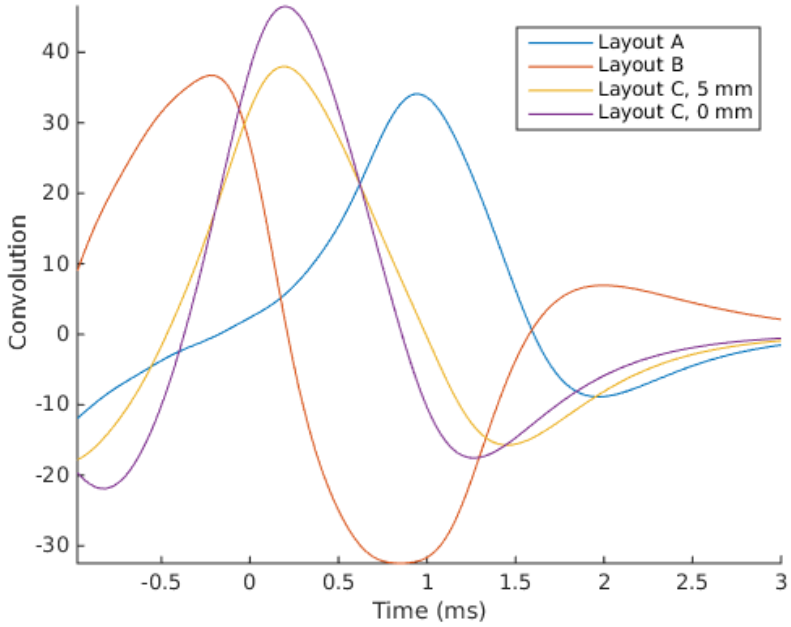

Figure 4.16: Convolution of the electric fields and the exponential decay function. Time constant $\tau = 300$ µs. With this time constant, the layout C is only 3% better than the layout B.

amounts [45]. Because of this, N52 is the strongest magnetic material that could be used in a mass-produced magnetic stimulation machine.

If we were to combine the previous improvements (the radius of 1.5 m, the frequency of 84 revolutions per second, and 0 mm distance between the magnets), the peak of the induced electric field would increase by multiplier 46.9, but the pulse duration would be reduced to 400 µs. The resulting peak would be 80.7 V/m, at the distance of 20 mm between the magnet and the brain.

According to figure 1.3, this is more than enough to cause both motor activity and sensations in a human wrist, if the distance between the nerve and the magnet's surface is 20 mm. Even a larger distance would suffice. The system would also be strong enough for the pain-reducement therapy performed by Smania *et al.* [20].

5 Conclusions

A magnetic block was built using 32 cubic permanent magnets with 20 mm side length. The block was attached to a lathe, and it was rotated at the radius of 40 cm and the rotation rate of 507 revolutions per minute. The magnets were placed on the block in such pattern that the rate of change of the magnetic field would be maximal at its center. The induced electric field was measured with a triangular wire loop.

The closest point of measurement was at 16.3 mm distance from the magnets' surface, and the peak of the induced electric field was 2.17 ± 0.07 V/m. At 20.0 mm distance, the peak of the induced electric field was 1.72 ± 0.06 V/m. The pulse duration was 4.1 ms at the 16.3 mm distance.

These fields are not strong enough for transcranial magnetic stimulation, but even with its current field strength, the prototype can be used to emulate transcranial current stimulation (tCS). Because this has different applications than TMS, it is desirable to increase the strength.

A pulse of this duration should induce an electric field in the order of 10–20 V/m to trigger an action potential in a human nerve cell. For practical applications, the field strength should be brought up to 50 V/m. There are some potential improvements. Placing the magnets closer to each other could increase the field strength by as much as 25%. Decreasing the distance between the magnet and the brain would increase the field, but a large improvement is not possible because the 20 mm distance is already similar to the thickness of the skull and the scalp.

To achieve significant improvements, the velocity of the magnet should be increased. This can be done by increasing the radius and the rotational frequency. It is reasonable to estimate that the radius could be increased to 150 cm before the stimulation machine becomes too large. This improvement alone would increase the field strength by 275%.

Increasing the rotational frequency tenfold would increase the induced electric field by tenfold. This might be possible, because there are materials that can safely withstand the centrifugal force. Limitations set by other factors, for example the size of the motor, were not considered.

After all suggested improvements, the electric field would peak at 80.7 V/m, at the distance of 20 mm between the magnet and the brain. The pulse duration would be 400 µs. This would be enough to trigger action potentials in the human nerve cells, and the new system could be used for the same applications as an electromagnet-based TMS system.

References

[1] A. T. Barker, R. Jalinous, and I. L. Freeston, "Non-invasive magnetic stimulation of human motor cortex," *The Lancet*, vol. 325, pp. 1106–1107, 1985.

[2] L. F. Haas, "Hans Berger (1873–1941), Richard Caton (1842–1926), and electroencephalography," *Journal of Neurology, Neurosurgery, and Psychiatry*, vol. 74, p. 9, 2003.

[3] P. M. Rossini and S. Rossi, "Transcranial magnetic stimulation: diagnostic, therapeutic and research potential," *Neurology*, vol. 68, pp. 484–488, 2007.

[4] M. Kobayashi and A. Pascual-Leone, "Transcranial magnetic stimulation in neurology," *The Lancet Neurology*, vol. 2, pp. 145–156, 2003.

[5] D. Purves, G. J. Augustine, D. Fitzpatrick, W. C. Hall, A.-S. LaMantia, J. O. McNamara, and L. E. White, *Neuroscience, Fourth Edition*. Sinauder Associates, Sunderland, Massachusetts, 2007.

[6] J. Ruohonen, *Transcranial magnetic stimulation: modelling and new techniques*. PhD thesis, Helsinki University of Technology, 1998.

[7] Alive Publishing Group (publisher), "Magnetic therapy: Using magnetic energy for health." `http://web.archive.org/web/20130624051103/http://www.alive.com/articles/view/18950/magnetic_therapy_using_magnetic_energy_for_health`.

[8] National Center for Complementary and Integrative Health, "Magnets for pain relief." `http://web.archive.org/web/20150203104920/https://nccih.nih.gov/health/magnet/magnetsforpain.htm`.

[9] M. H. Pittler, E. M. Brown, and E. Ernst, "Static magnets for reducing pain: systematic review and meta-analysis of randomized trials," *Canadian Medical Association Journal*, vol. 177, pp. 736–742, 2007.

[10] Wikimedia Commons, "Action_potential.svg." `http://upload.wikimedia.org/wikipedia/commons/4/4a/Action_potential.svg`.

[11] E. M. Wassermann, C. M. Epstein, U. Ziemann, V. Walsh, T. Paus, and S. H. Lisanby, *The Oxford Handbook of Transcranial Stimulation*. Oxford University Press, New York, 2008.

[12] S. Tringali, X. Perrot, L. Collet, and A. Moulin, "Repetitive transcranial magnetic stimulation: hearing safety considerations," *Brain Stimulation*, vol. 5, pp. 354–363, 2012.

[13] V. Nikouline, J. Ruohonen, and R. J. Ilmoniemi, "The role of the coil click in TMS assessed with simultaneous EEG," *Clinical Neurophysiology*, vol. 110, pp. 1325–1328, 1999.

[14] J. O. Nieminen, L. M. Koponen, and R. J. Ilmoniemi, "Experimental characterization of the electric field distribution induced by TMS devices," *Brain Stimulation*, 2015 (in press), DOI: 10.1016/j.brs.2015.01.004.

[15] J. D. Bourland, J. A. Nyenhuis, W. A. Noe, J. D. Schaefer, K. S. Foster, and L. A. Geddes, "Motor and sensory strength-duration curves for MRI gradient fields," in *Proceedings of the Society of Magnetic Resonance 4th Annual Meeting, New York*, vol. 1724, 1996.

[16] Wikimedia Commons, "Discharging_capacitor.svg." `http://commons.wikimedia.org/wiki/File:Discharging_capacitor.svg`.

[17] B. J. Recoskie, T. J. Scholl, and B. A. Chronik, "The discrepancy between human peripheral nerve chronaxie times as measured using magnetic and electrical stimuli: the relevance to MRI gradient coil safety," *Physics in Medicine and Biology*, vol. 54, pp. 5965–5979, 2009.

[18] N. Brunel and M. C. W. van Rossum, "Lapicque's 1907 paper: From frogs to integrate-and-fire," *Biological Cybernetics*, vol. 97, pp. 337–339, 2007.

[19] A. V. Peterchev, S. M. Goetz, G. G. Westin, B. Luber, and S. H. Lisanby, "Pulse width dependence of motor threshold and input-output curve characterized with controllable pulse parameter transcranial magnetic stimulation," *Clinical Neurophysiology*, vol. 124, pp. 1364–1372, 2013.

[20] N. Smania, E. Corato, A. Fiaschi, P. Pietropoli, S. M. Aglioti, and M. Tinazzi, "Therapeutic effects of peripheral repetitive magnetic stimulation on myofascial pain syndrome," *Clinical Neurophysiology*, vol. 114, pp. 350–358, 2003.

[21] P. M. Rossini, D. Burke, R. Chen, L. G. Cohen, Z. Daskalakis, R. D. Iorio, V. D. Lazzaro, F. Ferreri, P. B. Fitzgerald, M. S. George, M. Hallett, J. P. Lefaucheur, B. Langguth, H. Matsumoto, C. Miniussi, M. A. Nitsche, A. Pascual-Leone, W. Paulus, S. Rossi, J. C. Rothwell, H. R. Siebner, Y. Ugawa, V. Walsh, and U. Ziemann, "Non-invasive electrical and magnetic stimulation of the brain, spinal cord, roots and peripheral nerves: Basic principles and procedures for routine clinical and research application. An updated report from an I.F.C.N. committee," *Clinical Neurophysiology*, 2015 (in press), DOI: 10.1016/j.clinph.2015.02.001.

[22] A. A. Marino, E. Nilsen, A. L. Chesson Jr., and C. Frilot, "Effect of low-frequency magnetic fields on brain electrical activity in human subjects," *Clinical Neurophysiology*, vol. 115, pp. 1195–1201, 2004.

[23] G. B. Bell, A. A. Marino, A. L. Chesson, and F. Struve, "Electrical states in the rabbit brain can be altered by light and electromagnetic fields," *Brain Research*, vol. 570, pp. 307–315, 1992.

[24] G. B. Bell, A. A. Marino, and A. L. Chesson, "Frequency-specific responses in the human brain caused by electromagnetic fields," *Journal of the Neurological Sciences*, vol. 123, pp. 26–32, 1994.

[25] G. B. Bell, A. A. Marino, and A. Chesson, "Low-level EMFs are transduced like other stimuli," *Journal of the Neurological Sciences*, vol. 144, pp. 99–106, 1996.

[26] K. A. Jenrow, X. Zhang, W. E. Renehan, and A. R. Liboff, "Weak ELF magnetic field effects on hippocampal rhythmic slow activity," *Experimental Neurology*, vol. 153, pp. 328–334, 1998.

[27] V. V. Vorobyov, E. A. Sosunov, N. I. Kukushkin, and V. V. Lednev, "Weak combined magnetic field affects basic and morphine-induced rat's EEG," *Brain Research*, vol. 781, pp. 182–187, 1998.

[28] K. Heusser, D. Tellschaft, and F. Thoss, "Influence of an alternating 3 Hz magnetic field with and induction of 0.1 millitesla on chosen parameters of the human occipital EEG," *Neuroscience Letters*, vol. 239, pp. 57–60, 1997.

[29] H. Sonnier, O. V. Kolomytkin, and A. A. Marino, "Resting potential of excitable neuroblastoma cells in weak magnetic fields," *Cellular and Molecular Life Sciences*, vol. 57, pp. 514–520, 2000.

[30] G. Ruffini, F. Wendling, I. Merlet, B. Molaee-Ardekani, A. Mekonnen, R. Salvador, A. Soria-Frisch, C. Grau, S. Dunne, and P. C. Miranda, "Transcranial current brain stimulation (tCS): Models and technologies," *IEEE Transactions on Neural Systems and Rehabilitation Engineering*, vol. 21, pp. 333–345, 2013.

[31] M. Bikson, C. Hahn, S. A. Macuff, P. Minhas, A. Rahman, and J. K. Rice, "Voltage limited neurostimulation," 2014. US Patent 8,818,515.

[32] D. Reato, A. Rahman, M. Bikson, and L. C. Parra, "Effects of weak transcranial alternating current stimulation on brain activity: a review of known mechanisms from animal studies," *Frontiers in Human Neuroscience*, vol. 7, pp. 1–8, 2013.

[33] D. Liebetanz, F. Fregni, K. K. Monte-Silva, M. B. Oliveira, Â. A. dos Santos, M. A. Nitsche, and R. C. A. Guedes, "After-effects of transcranial direct current stimulation (tDCS) on cortical spreading depression," *Neuroscience Letters*, vol. 398, pp. 85–90, 2006.

[34] W. Paulus, "Transcranial electrical stimulation (tES – tDCS; tRNS, tACS) methods," *Neuropsychological Rehabilitation*, vol. 21, pp. 602–617, 2011.

[35] A. Datta, M. Elwassif, F. Battaglia, and M. Bikson, "Transcranial current stimulation focality using disc and ring electrode configurations: FEM analysis," *Journal of Neural Engineering*, vol. 5, pp. 163–174, 2008.

[36] R. J. Ilmoniemi, M. S. Hämäläinen, and J. Knuutila, "The forward and inverse problems in the spherical model," in *Biomagnetism: Applications & Theory*, Pergamon Press, New York, 1985.

[37] R. J. Ilmoniemi, "The triangle phantom in magnetoencephalography," *The Journal of Japan Biomagnetism and Bioelectromagnetic Society*, vol. 22, pp. 44–45, 2009.

[38] F. Gram, "Magnetic field at a distance from a bar magnet." `http://web.archive.org/web/20120220030524/http://instruct.tri-c.edu/fgram/web/Mdipole.htm`.

[39] e-Magnets UK, "Grades of neodymium." `http://web.archive.org/web/20130715200827/http://www.ndfeb-info.com/neodymium_grades.aspx`.

[40] J. O. Nieminen, L. M. Koponen, and R. J. Ilmoniemi, "An automatic, computer-controlled TMS-coil calibrator," *Clinical Neurophysiology*, vol. 124, pp. e163–e164, 2013.

[41] A. Thielscher and T. Kammer, "Electrical properties of two commercial figure-8 coils in TMS: calculation of focality and efficiency," *Clinical Neurophysiology*, vol. 115, pp. 1697–1708, 2004.

[42] M. Sekino, "s_mag.jpg." `http://web.archive.org/web/20150225090612/http://www.bee.t.u-tokyo.ac.jp/image/s_mag.jpg`.

[43] F. Cardarelli, *Materials Handbook: A Concise Desktop Reference*. Springer Science & Business Media, 2008.

[44] J. Malmivuo and R. Plonsey, *Bioelectromagnetism: Principles and Applications of Bioelectric and Biomagnetic Fields*. Oxford University Press, New York, 1995.

[45] Private communication with the customer service of Shenzen Smart Magnet Co., Ltd.